PHENIX Forward Spectrometer Upgrade for Nucleon Structure and Heavy Ion Physics

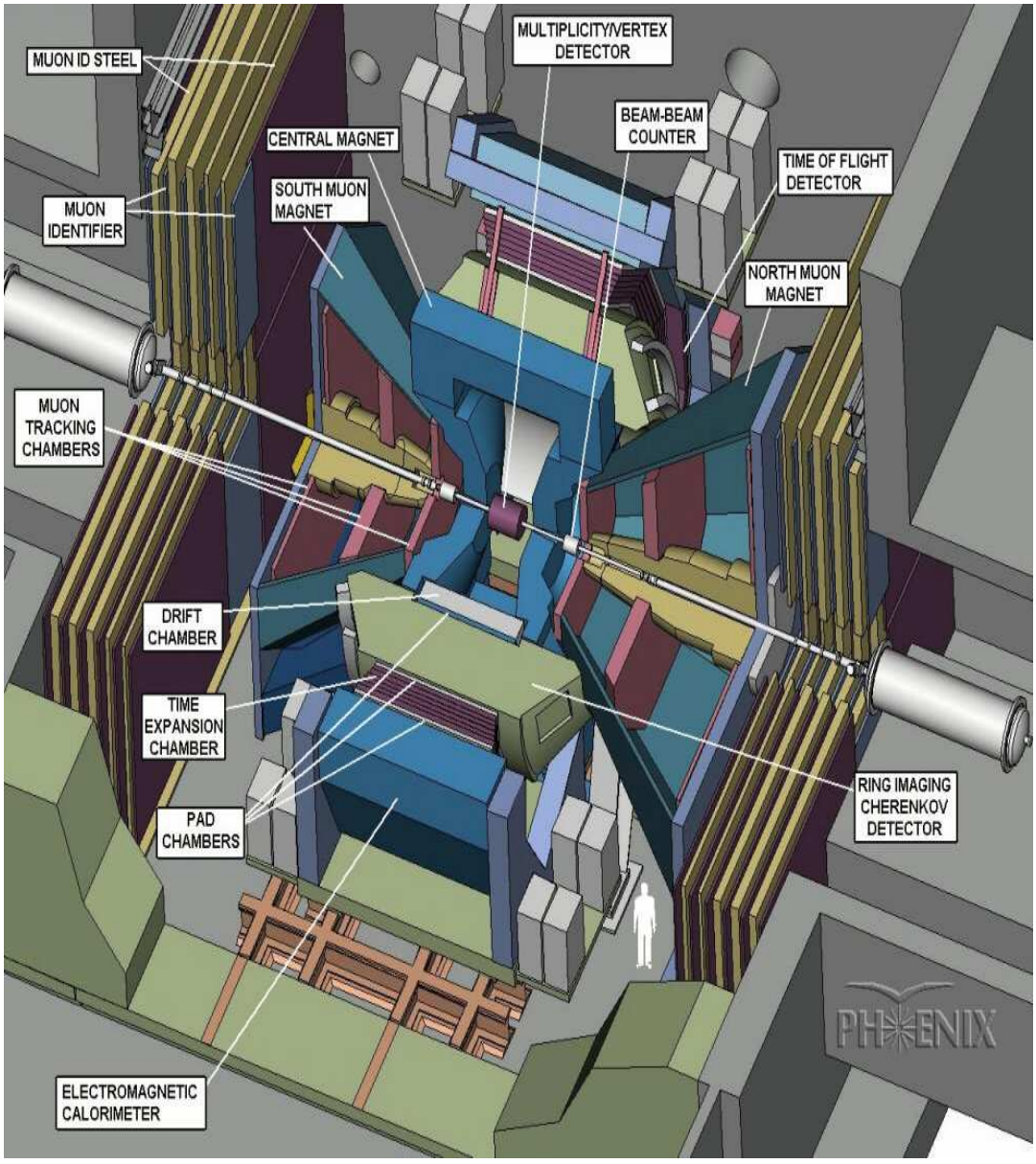

The PHENIX Detector

Brookhaven National Laboratory
Edward Kistenev, Pete Kroon, Mike Tannenbaum, Craig Woody

University of Colorado
Frank Ellinghaus, Ed Kinney, Jamie Nagle, Joseph Seele, Matt Wysocki

University of California at Riverside
Ken Barish, Stefan Bathe, Xinhua Li, Astrid Morreale, Richard Seto, Tim Hester, Alexander Solin

University of Illinois at Urbana Champaign
Mickey Chiu, Matthias Grosse Perdekamp, Hiro Hiejima, Alexander Linden-Levy Cody McCain, Jen-Chieh Peng, Joshua Rubin, Ralf Seidel

Iowa State University
John Lajoie, John Hill, Harold Skank, Gary Sleege

Kyoto University
Naohito Saito, Ken-ichi Imai, Kazuya Aoki, Kohei Shoji

Moscow State University
Mikhail Merkin, Alexander Voronin

Nevis Laboratory
Cheng Yi Chi

University of New Mexico
Doug Fields

RIKEN
Atsushi Taketani

RBRC
Gerry Bunce, Wei Xie

University of Tennessee
Vasily Dzhordzhadze, Ken Read

INFN Trieste
Andrea Vacchi, Valter Bonvicini

1. Introduction

A forward spectrometer upgrade is being proposed with the objective of introducing new detector capabilities and greatly enhancing present capabilities for PHENIX in the forward direction. These include detection of high momentum single muons, neutral pions, jets and single photons. This will add exciting new physics capabilities to the heavy ion and spin programs at RHIC and lead to pioneering measurements of nuclear effects on the gluon distribution function. This document outlines the physics possible with the forward calorimeter and instrumentation needed. It is designed to provide information to scientists who might have an interest in joining this project. The proposal has been presented for approval to the PHENIX Detector Council and Executive Council.

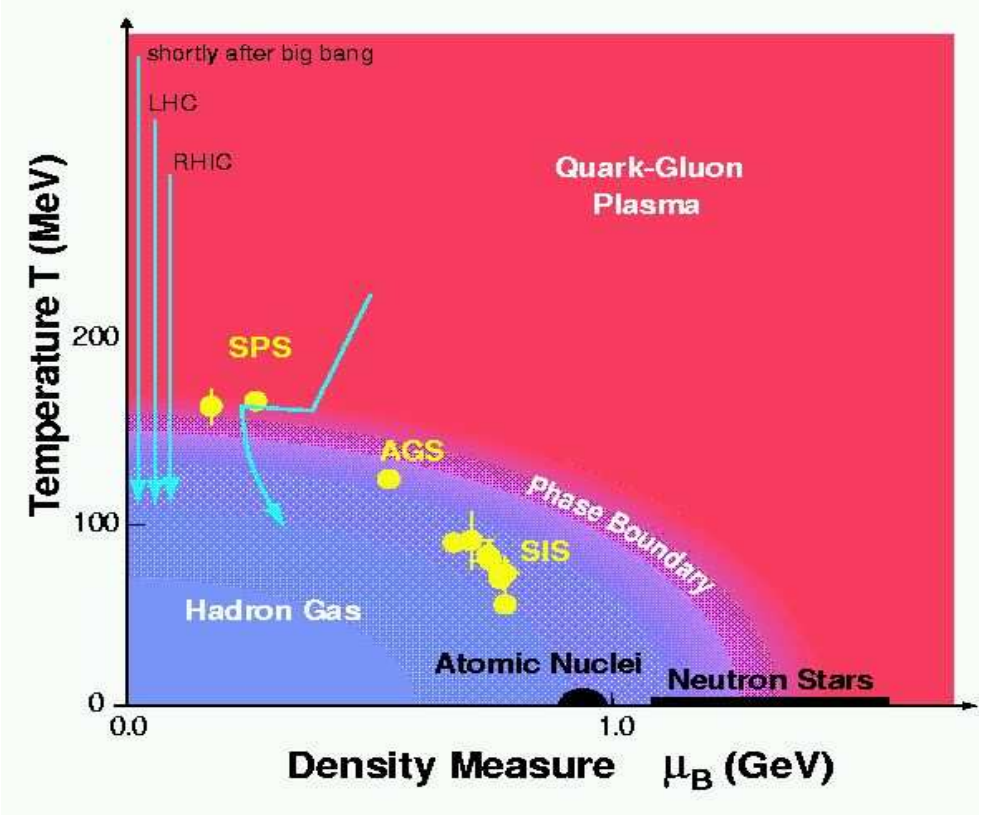

Fig. 1. Phase diagram of temperature vs nuclear density for nuclear matter. Shown is the boundary between the gas of hadrons and the deconfined state of quarks and gluons.

The Relativistic Heavy Ion Collider (RHIC) at Brookhaven National Laboratory (BNL) is the U.S. Department of Energy's forefront research facility for the study of the collisions of relativistic heavy ions and high-energy polarized protons. RHIC and a set of four detectors, BRAHMS, PHENIX, PHOBOS and STAR, were completed in 1999 and the physics program began in June 2000 with the study of Au-Au collisions. In July 2001 study of Au-Au collisions at the RHIC design energy of 100 GeV/nucleon began. Studies of collisions of 100 GeV polarized protons began in late 2002. RHIC runs are

conducted on a yearly basis with lengths typically of from 25 to 30 weeks.

RHIC was originally conceived for the study of the strong interaction at the highest accessible energy densities. The scientific objective is to produce new states of nuclear matter with very high temperatures and energy densities that could result in the formation of a new state of deconfined quarks and gluons called the Quark Gluon Plasma (QGP). RHIC is the logical successor to extensive heavy-ion programs at the AGS at BNL and the SPS at CERN and increases the accessible energy scale by one order of magnitude. Quantum Chromodynamics (QCD) predicts that as the temperature and/or baryon density of nuclear matter is increased there should be a transition to a deconfined phase (QGP). A phase diagram for nuclear matter is shown in Fig. 1 indicating the boundary between hadronic matter and the QGP. It is expected that at energies attainable with Au-Au collisions at RHIC it will be possible to exceed the transition temperature, produce the QGP and study it's properties, and study the nature of the phase transition between hadronic and quark matter.

At RHIC p-A or d-A collisions make it possible to study nucleon structure as a function of the nuclear environment at energy densities at least a factor of five higher than in previous experiments at FNAL or CERN. Forward production of inclusive hadrons, jets, direct photons or Drell-Yan pairs at small x(ion) in nucleon-ion collisions at RHIC will provide a new window for the observation of saturation phenomena expected at high parton number densities. In particular it may be possible to confirm or falsify the existence of the Color Glass Condensate (CGC) at high gluon densities prior to the arrival of e-A collisions at HERA or e-RHIC.

A major objective of the RHIC scientific program is to study the origin of the proton spin. It is well known that only 20 to 30 % of the nucleon spin can be described in terms of the spins of the three valence quarks. Other possible contributions are from the gluons, the sea quarks and orbital momenta of the valence quarks. The advent of modern QCD re-summation techniques and development of high energy polarized proton beams at RHIC allow the possibility of separating the role of the various contributions. These studies will complement experiments to study nuclear structure in deep inelastic scattering at SLAC, CERN, DESY and Jefferson Laboratory with unique capabilities to access polarized proton, quark and anti-quark distributions in the proton.

2. The RHIC Accelerator Complex

The RHIC is a two-ring superconducting hadron collider 3.8 km in circumference. A chain of hadron accelerators consisting of the Tandem Van de Graaff, the Booster and the Alternating Gradient Synchrotron (AGS) are used to inject heavy ions into the RHIC rings. For polarized protons the Tandem is replaced by the Proton Linac. The basic RHIC design parameters are shown in Table 1 of Ref. 1. The top energies for heavy-ion

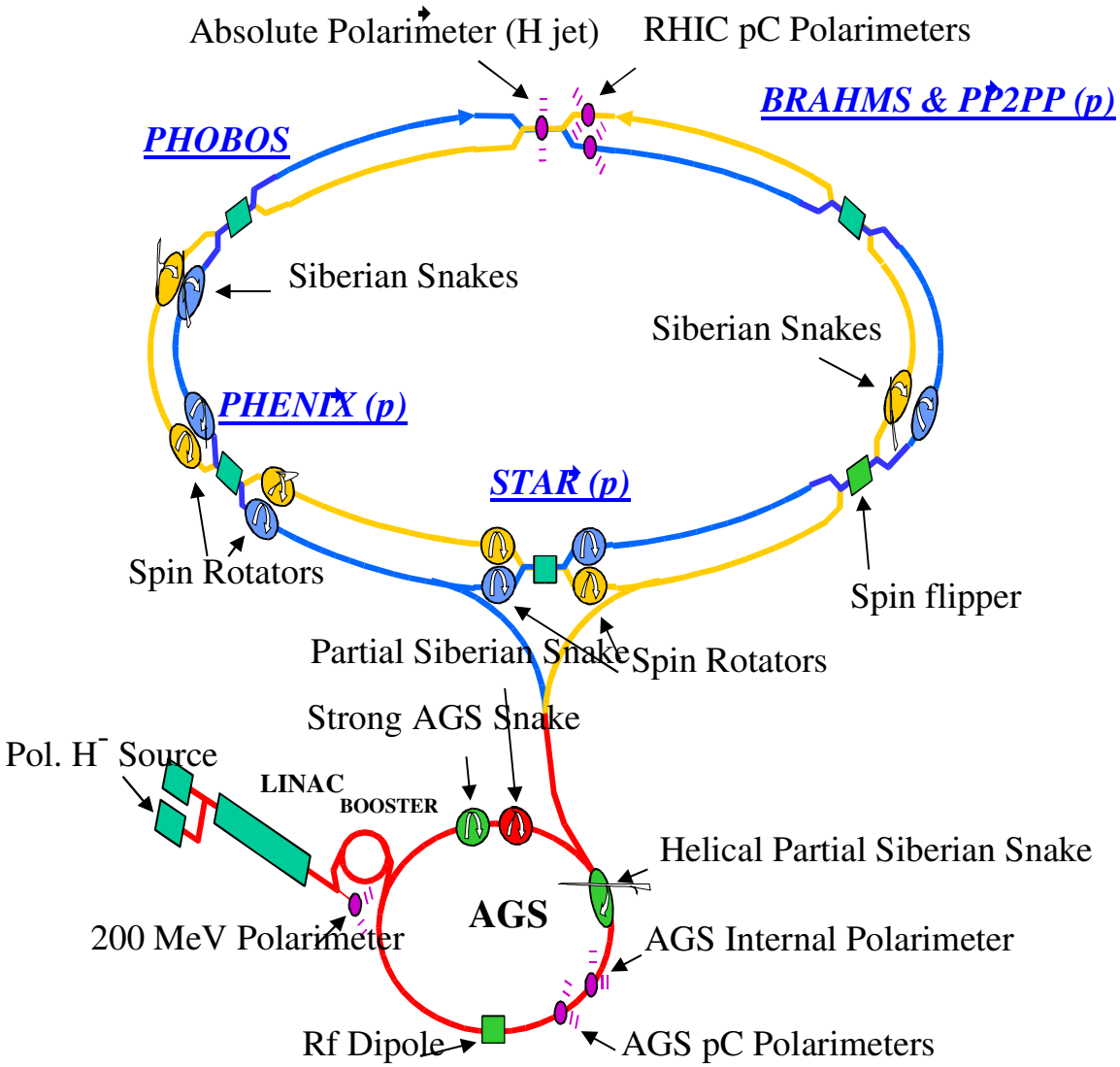

Fig. 2. Diagram of the RHIC and auxiliary accelerators. Shown are the Siberian Snakes, Spin Rotators and the four detectors.

beams (Au) and protons are 100 GeV/nucleon and 250 GeV, respectively. The RHIC rings are oriented to intersect with one another at six points along the circumference.
For heavy ions the electrons of the ions are successively stripped in each accelerating

stage until on exiting from the AGS the Au ions are completely stripped. Polarized protons are injected from the 200 MeV Proton Linac but it is difficult to maintain the polarization at high energies due to the many depolarizing resonances. A series of Siberian Snakes were installed in both the RHIC and the AGS to minimize polarization loss during acceleration. A RHIC design overview is given in Ref. 1 and an overview of RHIC capabilities for polarized protons is given in Ref. 2. The layout of Siberian Snakes and Spin Rotators is shown in Fig. 2.

An important parameter for performance of the RHIC accelerator is luminosity. The RHIC design peak luminosity was $9x10^{26}$ $cm^{-2}s^{-1}$ and $5x10^{30}$ $cm^{-2}s^{-1}$, respectively, for 100 GeV/nucleon Au-Au and 100 GeV polarized p-p collisions. The design peak luminosities for both beams were exceed in Run-4 reaching $15x10^{26}$ $cm^{-2}s^{-1}$ and $6x10^{30}$ $cm^{-2}s^{-1}$ for Au-Au and polarized p-p collisions, respectively. A primary goal for the future of RHIC is to upgrade the luminosity. In Run-4 a polarization for p-p of 40% was obtained. Recently RHIC has projected that for Run-6 in 2006 the targets for peak luminosity will be $25x10^{26}$ $cm^{-2}s^{-1}$ and $22x10^{30}$ $cm^{-2}s^{-1}$, respectively, for Au-Au and p-p collisions. The goal for Run-6 p-p polarization is 65%. Further in the future cooling of heavy ion beams would be needed to increase luminosity due to the strong intra-beam scattering.

3. The PHENIX Detector

The PHENIX detector is designed to perform a broad study of A-A, d-A, and p-p collisions to investigate nuclear matter under extreme conditions. Designing for the needs of the heavy-ion and polarized-proton programs has produced a detector with unparalleled capabilities. PHENIX measures electron and muon pairs, photons, and hadrons with excellent energy and momentum resolution. The PHENIX detector utilizes a variety of detector technologies. It uses global detectors to characterize the collisions, a pair of central spectrometers at mid-rapidity to measure electrons, hadrons, and photons, and a pair of forward spectrometers to measure muons. Each spectrometer has a large geometric acceptance of about one steradian and excellent particle identification.

The rapidity, azimuthal coverage and other features of the PHENIX subsystems are given in Table 1 of Ref. 3 and 2D drawings of the PHENIX detector with the major subsystems labeled are shown in Fig. 3. The east and west central arms are centered at zero rapidity and the north and south forward arms have full azimuthal coverage. The global detectors measure the start time, vertex and multiplicity of the interactions. The performance of the PHENIX detector is summarized in Table 3 of Ref. 3.

3.1. Global Detectors

In order to characterize the nature of an event following a heavy ion collision, three global detectors are employed. They consist of Zero-Degree Calorimeters (ZDC), Beam-Beam Counters (BBC) and the Multiplicity-Vertex Detector (MVD). A pair of ZDCs [4] detect neutrons from grazing collisions and form a trigger for the most peripheral collisions. The ZDC is used by all four RHIC detectors. A pair of BBCs [5] provide a measure of the time-of-flight of forward particles to determine the time of a collision, provide a trigger for the more central collisions and provide a measure of the collision position along the beam axis. The MVD [5] provides a more precise determination of event position and multiplicity and measures fluctuations of the charged particle distributions. It is composed of concentric barrels of silicon-strip detectors and endcaps made of silicon pads.

3.2. Central Spectrometers

The magnetic field for the central spectrometer is supplied by the central magnet [6] that provides an axial field parallel to the beam and around the interaction vertex. The central arms consist of tracking systems for charged particles and electromagnetic calorimetry. The calorimeter [7] is the outermost subsystem on the central arms and provides measurements of both photons and energetic electrons. A lead-scintillator (PbSc) calorimeter is used for good timing and a lead-glass (PbGl) calorimeter gives good energy resolution.

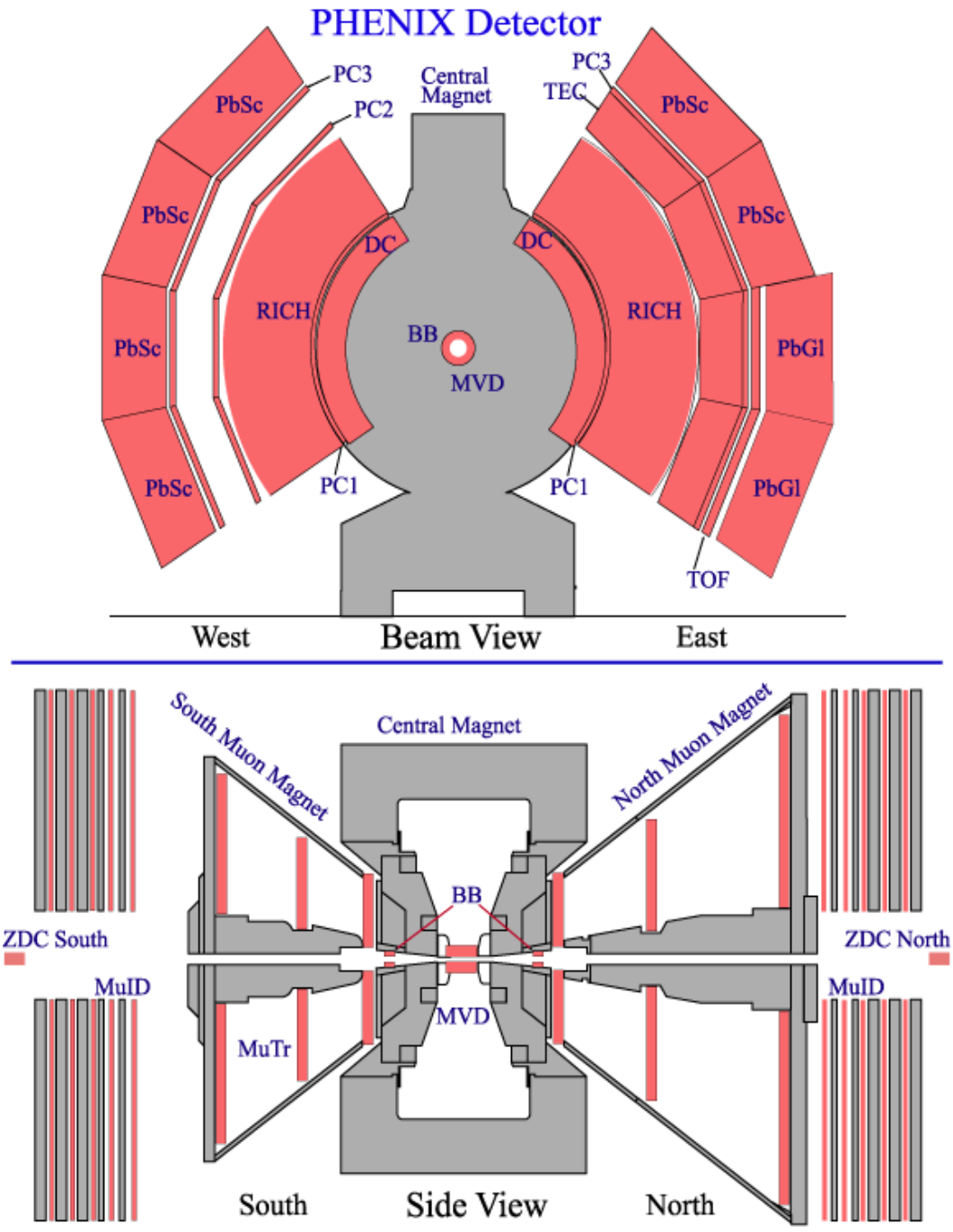

Fig. 3. A beam view (top) and side view (bottom) of the PHENIX detector in it's run-3 configuration. The designations for the various subsystems are explained below.

The tracking system uses three sets of Pad Chambers (PC) [8] to provide precise three-dimensional space points needed for pattern recognition. The precise projective tracking of the Drift Chambers (DC) [8] is the basis of the excellent momentum resolution. A Time Expansion Chamber (TEC) [8] in the east arm provides additional tracking and particle identification. The Time-of-Flight (ToF) and Ring-Imaging CHerenkov (RICH)

detectors also provide particle identification [9]. The 85 ps timing resolution of the ToF allows separation of kaons from pions up to 2.5 GeV/c and proton identification out to 5 Gev/c. For p-p running the ToF timing resolution would be poorer than for heavy ions due to a reduced number of particles in the BBC. The ToF timing is improved by the use of a T0 counter [9] outside the barrel of the MVD. This is needed for p-p and p-A experiments. The RICH provides separation of electrons from the large number of copiously produced pions. Using information from the RICH, the TEC and the electromagnetic calorimeter it is possible to reject pion contamination of identified electrons to one part in 10^4 over a wide range of momentum.

3.3. Muon Spectrometers

The two forward muon spectrometers [10] give PHENIX acceptance for J/ψ decaying into dimuons at rapidities of $-2.25 < y < -1.15$ for the south arm and $1.15 < y < 2.44$ for the north arm. Each spectrometer is based on a Muon Tracker (MuTr) inside a radial magnetic field [6] followed by a Muon Identifier (MuID), both with full azimuthal acceptance. The MuTrs consist of three stations of multi-plane drift chambers that provide precision tracking. The MuIDs consist of alternating layers of steel absorbers and low resolution tracking layers of streamer tubes of the Iarocci type. With this combination the pion contamination of identified muons is typically 3×10^{-3}.

3.4. Electronics and Computing

PHENIX selects and archives events of potential physics interest at the maximum rate consistent with the available RHIC luminosity. The channel count for the PHENIX detector is large and details of the various subdetectors is given in Table 2 of Ref. 3. Custom Front-End Electronics (FEE) were designed for the PHENIX subsystems. Signals from the FEEs [11] are transported by optical fibers to the level-1 trigger [11] that processes signals from a number of subsystems to make a decision. The trigger does the first on-line screening of events in PHENIX. It is a beam-clock parallel-pipeline system that uses multiple Local Level-1 (LL1) algorithms pertaining to the fastest PHENIX detectors, followed by a Global Level-1 (GL1) system that processes encoded LL1 reduced-bit data to issue up to 32 triggers. The LL1 algorithms operate on raw data to produce a first estimate of the number of electrons, photons, muons and hadrons as well as the electromagnetic energy and event vertex. These LL1 systems process input data at a rate exceeding 20 Gbit/s. The latency of the entire system is less than 40 beam crossings. The level-1 trigger is implemented using custom-designed 9U VME-P format boards and reprogrammable FPGA logic. The timing of the above operations is coordinated by a master timing system [11] that distributes the RHIC clocks to granule timing modules that communicate with the FEEs. A schematic diagram of the level-1 trigger is shown in Fig. 4.

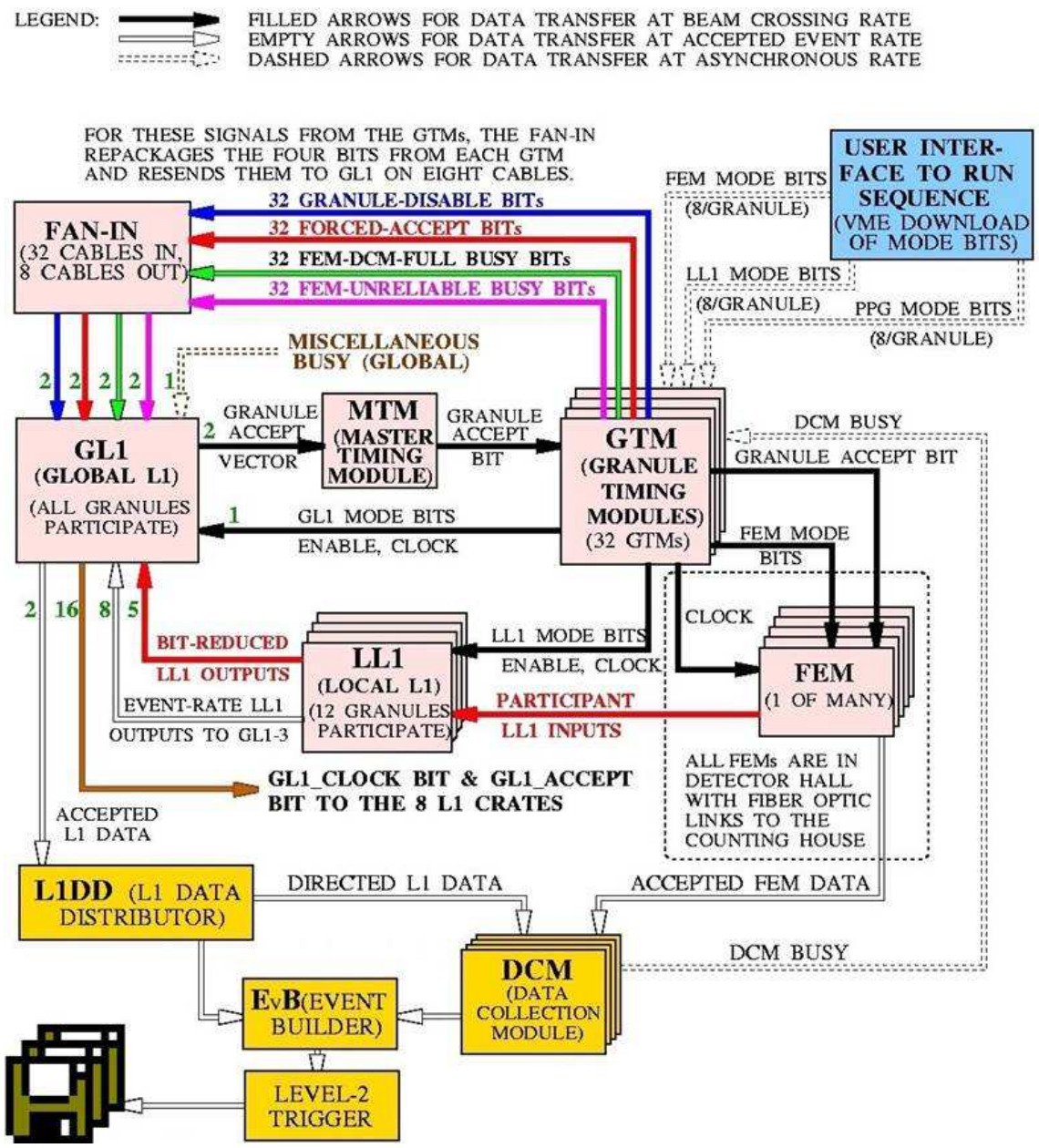

Fig. 4. A schematic diagram of the level-1 trigger and it's interaction with other elements of the PHENIX on-line timing system.

In order to study the rare event physics for which PHENIX was designed, it is necessary to have a higher level of event rejection than possible with the level-1 trigger alone. Therefore a level-2 software trigger [11] that makes its selection after a complete event is assembled was developed. Once the level-1 trigger accepts an event, the data from the various subsystems is routed via fiber-optic cable to the data collection modules [11] that interact with the subsystems by means of daughter cards that format and zero-suppress the data. Data packets are generated by digital signal processors and sent to event

builders [11] that assemble the events in their final form. The control and monitoring of the electronics and triggering is handled by the On-Line Computing System (ONCS) [12]. ONCS configures and initializes the on-line system, monitors and controls the data flow and interlocks the data acquisition process with the slow controls systems. After the data is collected the off-line system [12] provides event reconstruction, data analysis and information management. It provides the tools to convert raw data into physics results.

4. The PHENIX Physics Program

The PHENIX detector is designed to perform a broad study of A-A, d-A, and p-p collisions to investigate nuclear matter under extreme conditions. A wide variety of probes, sensitive to all timescales, are used to study systematic variations with species and energy and to measure the spin structure of the nucleon. A prime goal for experiments with heavy ion beams is to produce a deconfined state of nuclear matter (QGP) and study it's properties. This is thought to be the state of the universe a μs after its birth in the "big bang". Measuring leptons and photons probes the QGP phase directly, while studying the copiously produced hadrons gives information on the later hadronization of the QGP.

QCD predicts that heavy nuclei colliding at ultrarelativistic energies will undergo a phase transition from hadronic matter to the QGP (see Fig. 1). This process can be thought of as proceeding through a series of steps from the initial collision through QGP formation (deconfinement) and possible chiral symmetry restoration. The QGP would thermalize followed by expansion and cooling leading to hadronization. PHENIX is able to probe each phase of the above process by virtue of its ability to study the rare processes involving photons, electrons and muons as well as the predominant hadronic production. The experiment has a high rate capability and fine granularity.

Direct photons and lepton pairs which emerge from the collision with a minimum of final state interaction are sensitive to the full time evolution from the initial state through thermalization. The capability to measure direct photons over a wide range of p_T is unique to PHENIX and is important for relating their momentum to the temperature of the emitting source. Jets from the hard scattering of constituent quarks and gluons are produced in the initial state and are sensitive to the properties of the medium during the evolution so that a significant modification of the structure of the jet is expected if a QGP is formed. PHENIX studies the deconfined state and Debye screening by observing the yields of the J/ψ and ψ' relative to that of the Υ. Chiral symmetry restoration is predicted to result in the reduction of quark masses and possible changes in the lifetime and width of the ϕ and possibly the ρ and ω. All of the above vector mesons are studied by observation of their decays into lepton pairs.

After hadronization the expansion of the fireball is studied by measurement of Hanbury-Brown-Twiss correlations and the coalescence probabilities of various nuclei and anti-nuclei give insights into the space-time evolution of the collision. Precision time of flight (ToF) allows measurement of the identified charged hadron spectrum over a wide p_T range. Many of the above signals can also be produced from interactions between particles in hot hadronic matter. It is thus necessary to understand the purely hadronic effects. For this reason PHENIX studies the above signals using p-p and p-A collisions to gain a better understanding of effects distorting signals from the QGP.

One of the unique capabilities of the RHIC accelerator complex is the ability to collide any pair of nuclei. It is thus possible to study for the first time p-A collisions at very high energy in a collider geometry. For two reasons p-A or d-A collisions are important. First, they serve as a a baseline measurement for the A-A program, providing the important null hypothesis check for new phenomena as was dramatically shown when hadron suppression was not observed at midrapidity in d-Au collisions, in sharp contrast to the factor of 5 suppression seen in central Au-Au collisions. Second, p-A collisions are interesting since recent theoretical advances have pointed to a new region of saturated parton distributions (CGC) where the gluons are treated classically and reasonably robust calculations can be done. Hints of saturation have been seen at HERA and more recently in data from BRAHMS and PHENIX's muon spectrometers. Study of this region and the CGC is important in that it may provide the initial state for the formation for the QGP being studied in A-A collisions. In addition studies may enhance our understanding of the topics of shadowing and proton fragmentation.

A major goal of the PHENIX experiment is to measure the spin structure of the nucleon. RHIC accelerates beams of polarized protons up to 250 GeV with polarizations up to 50%. Work of the EMC [13] collaboration and others indicated that the fraction of the proton spin carried by the quarks was only about half of the expected value. PHENIX studies the gluon polarization by measuring high p_T prompt photon production using the highly segmented EM Calorimeter to minimize interference from photons from π^0 decays. The anti-quark polarization is measured by observing the parity violating asymmetry for W production. The W particles are identified by the detection of muons or electrons with $p_T > 20$ GeV/c using the PHENIX north and south muon arms or the central spectrometer, respectively.

5. PHENIX Highlights and Discoveries

Below we highlight some of the discoveries made during the first three years of operation of the PHENIX detector. Collisions studied were Au-Au at √s=130, 200 GeV/nucleon dAu at √s = 200 GeV/nucleon and polarized p-p at √s=200 GeV. Below a discussion of highlights in the heavy ion program is followed by a discussion of the spin (p-p) program.

5.1. Highlights from the PHENIX Heavy Ion Program

In order to interpret the results from the collisions of heavy nuclei an important first step was to establish a set of control parameters N(part) and N(coll) that refer to the number of particles that interact and the number of binary collisions that occur, respectively, and to establish experimental methods for extracting them. A combination of Zero-Degree Calorimeters (ZDC) and Beam-Beam counters (BBC) were used to define centrality classes which were then used with Glauber modeling [14] to extract N(part) and N(coll). The first PHENIX publication [15] illustrates the use of these parameters for determining charged particle multiplicity for √s 130 GeV Au-Au collisions.

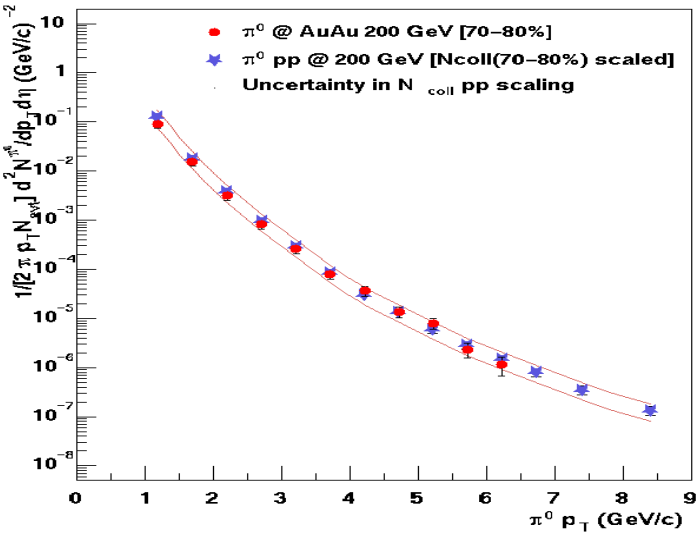

Fig. 5. A comparison of the yields of π^0s for Au-Au peripheral and p-p collisions at √s=200 GeV. The yield results are scaled by the number of binary collisions.

A major emphasis was to test the production of many different types of particles as a function of the number of binary collisions. Relatively rare processes should scale as the number of binary nucleon-nucleon collisions. This was studied for Au-Au, d-Au and p-p collisions at a number of different impact parameters. For most situations binary scaling was found to be valid as for example in the case of π^0 production in Au-Au peripheral collisions. In Fig. 5 a comparison with π^0 production in p-p collisions is shown.

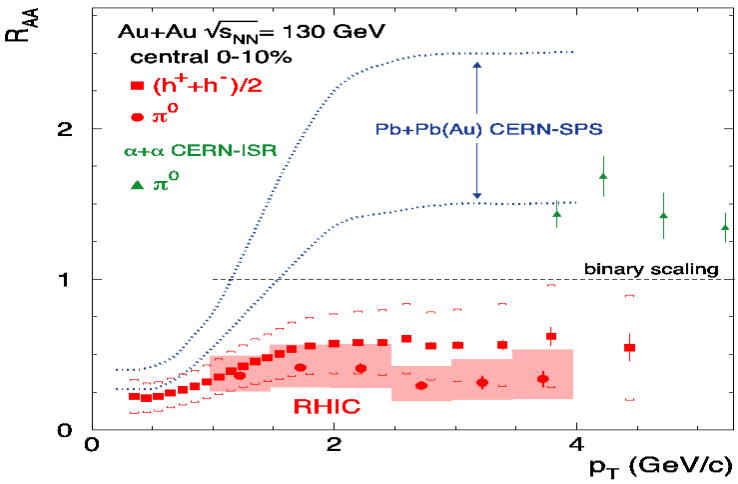

Fig. 6. Illustration of the suppression of hadrons with large p_T Au-Au central collisions at $\sqrt{s}$ = 130 GeV relative to N(coll) scaling.

An important discovery at PHENIX was the suppression [16] in central Au-Au collisions of hadrons with large transverse momentum relative to the predictions of binary scaling. The results are shown in Fig. 6. This variation of the Au-Au results from binary scaling hints at the formation of a state of dense hadronic matter that suppresses the hadronic yield. To test this hypothesis d-Au collisions were studied [17]. In this case an absence of suppression for high transverse momentum hadrons was observed. Comparison with the Au-Au data is shown in Fig. 7.

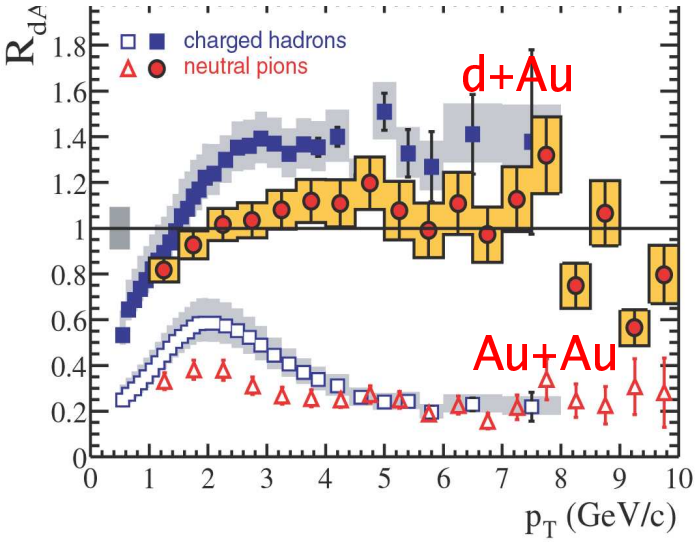

Fig. 7. Comparison of results for d-Au and Au-Au for high p_T charged hadrons and π^0s.

In contrast to the Au-Au results an absence of suppression in d-Au collisions is observed. Using the combined results on p-p, d-Au and Au-Au, it is clear that all processes that should exhibit binary scaling in central collisions of heavy projectiles do not, thus we have observed a new behavior for nuclear matter at RHIC. Possible explanations include

suppression of low-x gluons in the initial state or enhanced energy loss in a new state of nuclear matter. An important feature of the above discovery was the availability of p-p data at 200 GeV as a reference for the π^0 yields

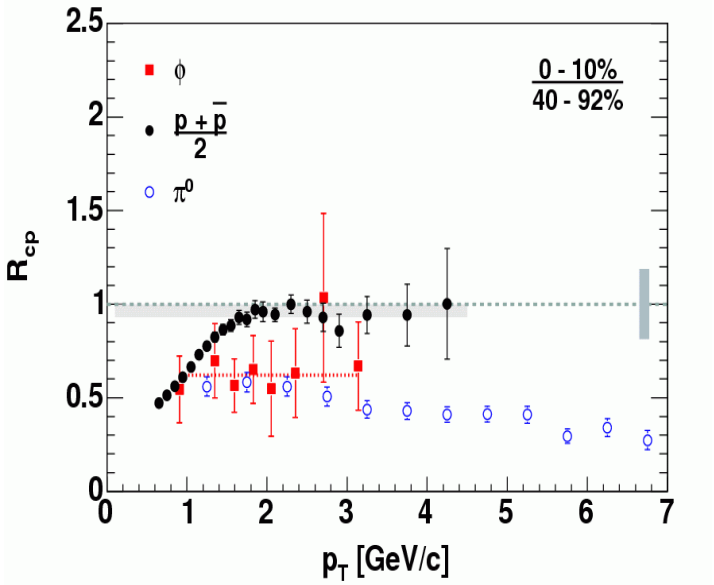

Fig. 8. The results from PHENIX indicate little suppression of baryons compared in the p_T range from 2 to 5 GeV/c. The π^0s are suppressed.

An interesting experimental finding is that at intermediate transverse momenta baryons are much less suppressed than mesons. This has been shown to be true at PHENIX for protons and anti-protons (as shown in Fig. 8) and at STAR for lambdas and anti-lambdas. Recombination is a possible explanation for different behavior of mesons and baryons. It provides a natural explanation for the spectrum of charged hadrons and the p/π ratios. This requires a thermalized partonic phase which might possibly be called the QGP. Also the flow anisotropy parameter v_2 should be different for a hadronic as opposed to a partonic medium. Deviations of v_2 for particles with transverse momenta greater than 2.5 GeV from the predictions of hydrodynamics also point to the possible formation of a partonic medium.

5.2. Highlights from the PHENIX Spin (p-p) Program

The goals of the PHENIX Spin Program are to make precision measurements of the gluon structure of the proton and of the spin structure of the gluon and sea-quark distributions of the proton. This is being carried out by experiments on p-p collisions with polarized protons. The first step in this program was to measure the invariant cross section for inclusive π^0 production in p-p collisions at $\sqrt{s}$ = 200 GeV. The measurements were made at midrapidity ($|\eta|< 0.35$) over a p_T range of $1<p_T<14$ GeV/c. This was carried out in Run-2 and the results have been published[18].

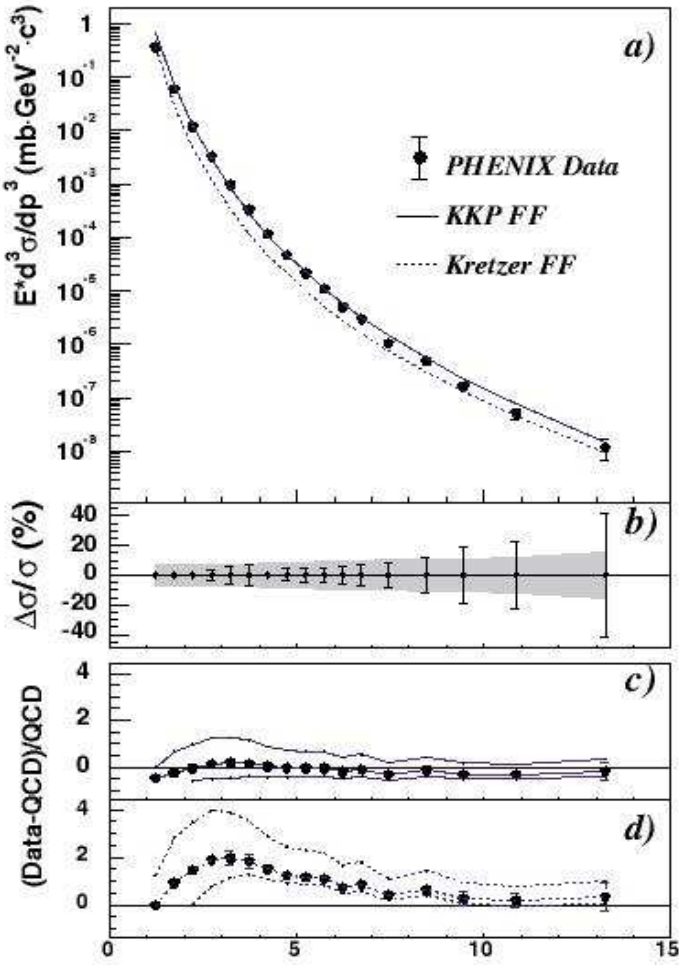

Fig. 9. (a) The invariant differential cross section for inclusive π^0 production and the results from NLO pQCD calculations using the KKP (solid line) and Kretzer (dashed line) sets of fragmentation functions. (b) The relative statistical (points) and point-to-point systematic (band) errors. (c),(d) The relative difference between the data and the theory using (c) KKP and (d) Kretzer fragmentation functions. With scales of $p_T/2$ (lower curve) and p_T and $2p_T$ (upper curve).

Using a sample of minimum bias events and a sample of events from the high-p_T trigger, the cross section for π^0 production was determined. The results are shown in Fig. 9 where they are compared with NLO pQCD calculations. As can be seen from the figure the results are consistent with a calculation using the Kniehl-Kramer-Potter (KKP) set of fragmentation functions [19] that give better agreement than a calculation with the Kretzer [20] set of functions. The difference is mainly in the gluon-to-pion fragmentation function (D^{π}_{g}) which is greater in the KKP set. Our data are the first from a hadron experiment from which an unambiguous conclusion about D^{π}_{g} may be drawn.

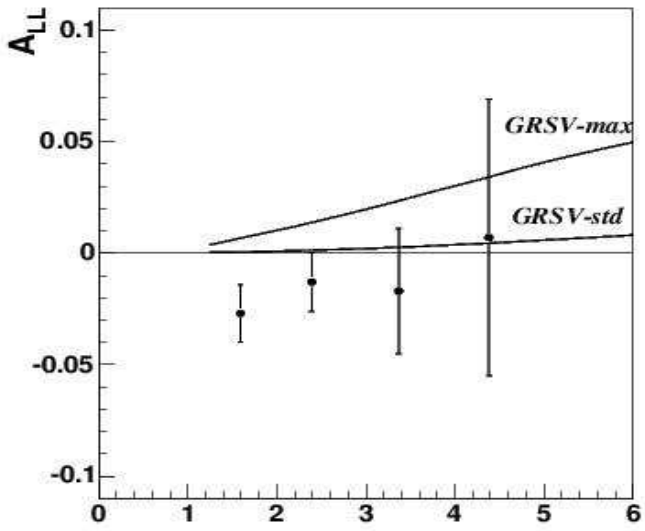

Fig. 10. The measured $A_{LL}(\pi^0)$ vs mean p_T of π^0s in each bin. Two theoretical calculations based on NLO pQCD are shown for comparison. See [nn] for details.

Data on p-p collisions from Run-3 were used to measure the double longitudinal spin asymmetry A_{LL} by inclusive π^0 production at $\sqrt{s}$ = 200 GeV. The average beam polarization was 27%. These measurements were the first in a program to study the longitudinal spin structure of the proton with strongly interacting probes at collider energies [21]. In p-QCD A_{LL} is directly sensitive to the polarized gluon distribution function in the proton through gluon-gluon and gluon-quark subprocesses. The results of the measurement for A_{LL} are shown in Fig. 10 along with two theoretical curves based on two different NLO pQCD calculations using different assumptions for the gluon polarization. The best fit GRSV-std is based on the best global fit to inclusive DIS data. The measured asymmetry is small.

The above measurements using polarized protons constituent an important confirmation of the theoretical foundations for the RHIC spin program. The results also provide confidence in going forward with spin measurements via hadronic channels. It is clear that we have just begun to explore the nature of the proton spin using polarized p-p collisions. RHIC and PHENIX present a unique and unprecedented opportunity to learn much more about the origin of the proton spin.

We end this discussion of the early discoveries at PHENIX and RHIC with a quote by Urich Heinz at the PANIC-02 conference. "But much more is to come, only now, with RHIC finally running at full energy and luminosity it is possible to address such hallmark measurements as thermal dilepton and direct photon emission and heavy quarkonium production, all of which play crucial roles in the early diagnostics of the QGP which we are apparently mass producing at RHIC. While trying to solve the HBT puzzle and to quantitatively understand jet quenching, we are looking forward to these high-luminosity measurements and any surprises they may bring"

6. Physics with the PHENIX Forward Spectrometer

6.1. Spectrometer Introduction

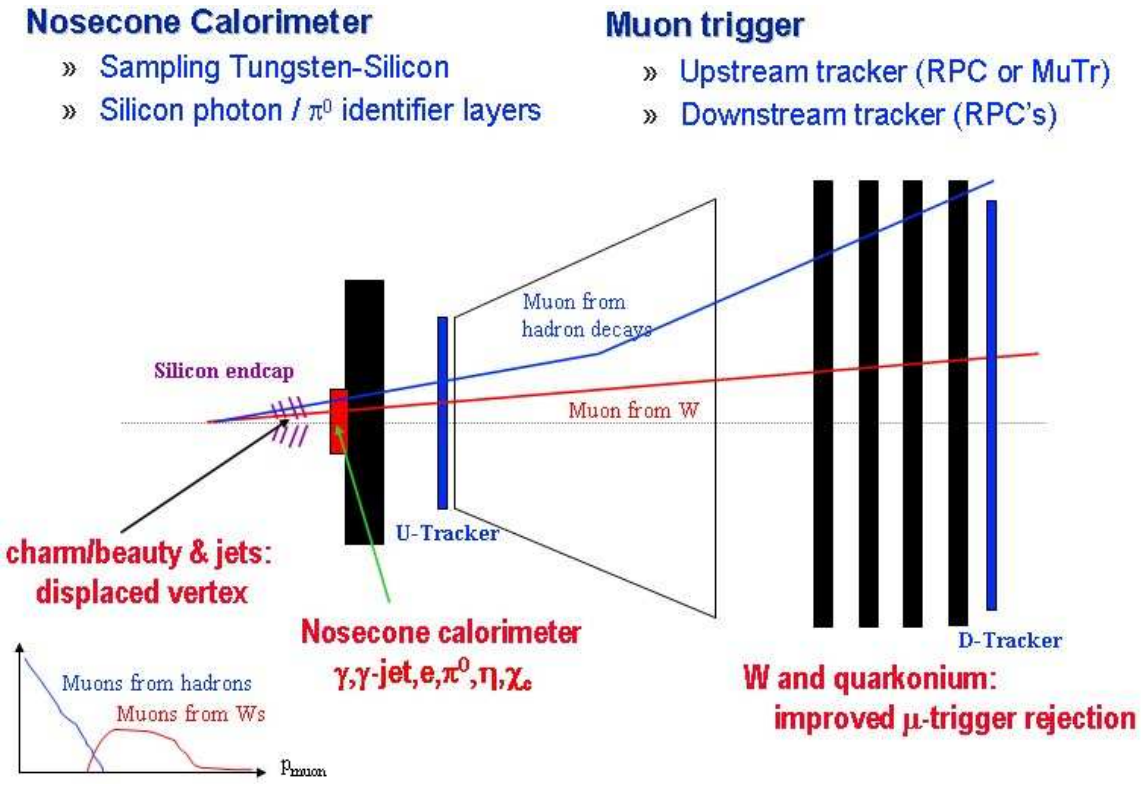

Fig. 11. A diagram for the proposed PHENIX forward spectrometer. The Resistive Plate Chambers (RPCs) that provide signals for a muon trigger are shown in blue and designated as U-tracker and D-tracker. The NCC is shown in red. All are centered with the beamline. Some of the physics measurements possible with the upgrade are listed.

The proposed PHENIX upgrade for a forward spectrometer is shown diagrammatically in Fig. 11. The two principal components are a muon trigger that processes signals from the RPCs and a NCC. The RPCs provide information to the muon trigger for the high luminosities proposed for the RHIC upgrade and improves rejection for beam and collision related backgrounds. This will be important for detection of W particles and quarkonium. The NCC is a W-Si sampling spectrometer with both an electromagnetic and a shallow hadronic component. It will cover 0.9<| |<3.0and expand kinematic coverage for jets, inclusive ^{0}s, electrons and forward photons to forward rapidities.

6.2. A-A Physics

The production of quarkonia in nuclear collisions is of fundamental importance because

these states are sensitive to both the gluon distribution of the initial state nuclear wave function and by virtue of their relatively long formation time to the ensuing dense partonic media. The formation time of the precursor heavy quark pair is given by the heavy quark mass and is 0.1 fm/c. In order to form a bound state the precursor state grows to the size of the physical quarkonia over a time scale given by the relative momentum of the heavy quarks in the bound state 1 fm/c. During the evolution of the precursor the surrounding nuclear medium can influence the formation of the bound state quarkonia by color screening the attractive potential between the heavy quarks [22], thus leading to the suppression of the formation of heavy quarkonia and nuclear induced reactions.

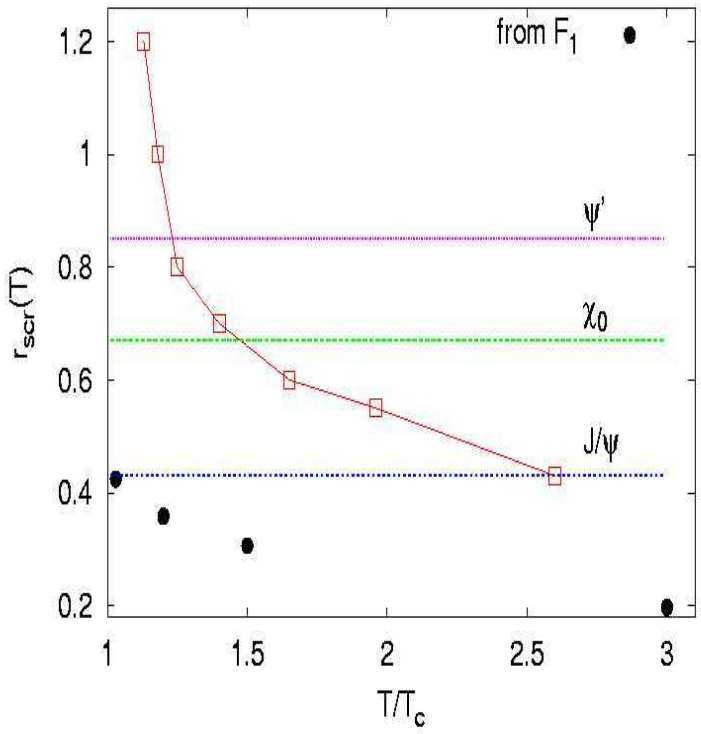

Fig. 12. The screening radius for various quarkonia states vs temperature from finite temperature QCD.

Efforts have been made to calculate the temperature dependence of the dissolution of heavy quark bound states using finite temperature QCD on the lattice. Fig. 12 shows the screening radius from the lattice versus temperature and the radii of 1S, 2S and 1P quarkonia. In contrast to earlier results based upon modifications to the heavy quark potential which predicted the J/ψ to melt at around the critical temperature for transition to a QGP [23], current predictions indicate the J/ψ persists until 2.5 times the critical temperature and the more deeply bound Upsilon (1S) will persist to temperatures well beyond that.

The suppression of the production of quarkonia can plausibly be attributed to nuclear effects other than the proposed suppression by dynamic color screening from a hot QGP. The most straightforward method to disentangle competing effects is to measure as many quarkonia states as possible. Fig. 13 shows the x_F dependence of suppression of scaling as measured by E866 at Fermilab. [24] At moderate values of x_F the difference between the suppression of 1S and 2S quarkonia is indicative of different nuclear absorption cross sections as expected based upon the factor of 2 difference in the size of the bound states. [25] As with precursor absorption in cold nuclear matter measuring multiple quarkonia states and connecting the observed suppression pattern with theory will help in unambiguously attributing an observed suppression pattern to the formation of a deconfined medium.

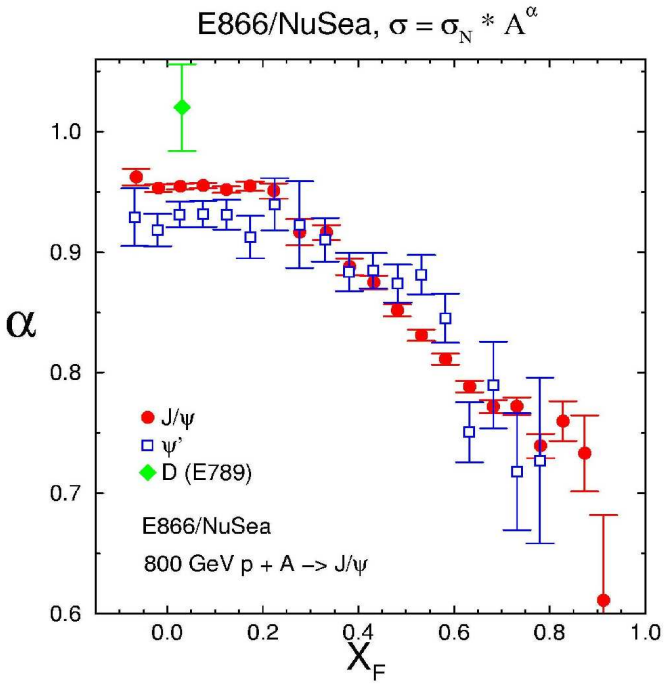

Fig. 13. x_F dependence of suppression of scaling as measured by E866 at Fermilab.

The proposed NoseCone Calorimeter (NCC) has the potential to extend the measurement of quarkonia at RHIC to include the P wave quarkonia, χ_c states via their radiative decay χ_c--> γ J/ψ. The χ_{c1} and χ_{c2} states are produced with cross sections commensurate with that of the J/ψ and their radiative decay channels have appreciable branching fractions (0.27 and 0.17 respectively). The measurement of χ_{c0} is precluded by the small branching fraction (~0.01) of its radiative decay. The PHENIX muon spectrometer has pseudo-rapidity coverage 1.2< |η|<2.2(2.4) in the south (north) muon arms respectively. The photon from the radiative decay of χ_c has a small relative momentum to that of its parent and therefore the proposed NCC has good acceptance (58%) for associated with J/ψ that are in the acceptance of the muon spectrometer.

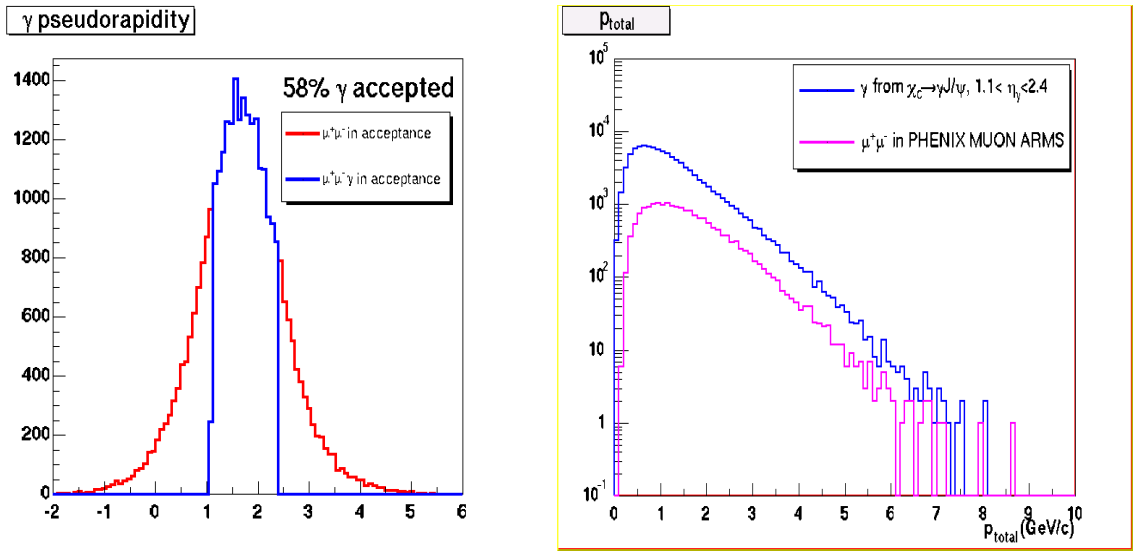

Fig. 14. The acceptance of γ associated with an accepted J/ψ (left) and the total momentum of the accepted γ (right).

Fig. 14 shows the acceptance of γ associated with an accepted J/ψ and the total momentum of accepted γ. The resolution for J/ψ in the current PHENIX muon spectrometer is limited by multiple-scattering and energy loss fluctuations in the hadronic absorber that exists between the spectrometer and the primary collision. It has been shown with a fast Monte-Carlo that the resolution of the reconstruction of χ_c for any reasonable range of calorimeter energy resolution is dominated by the angular resolution of the reconstructed J/ψ. Fig. 15 shows the invariant mass distribution of reconstructed

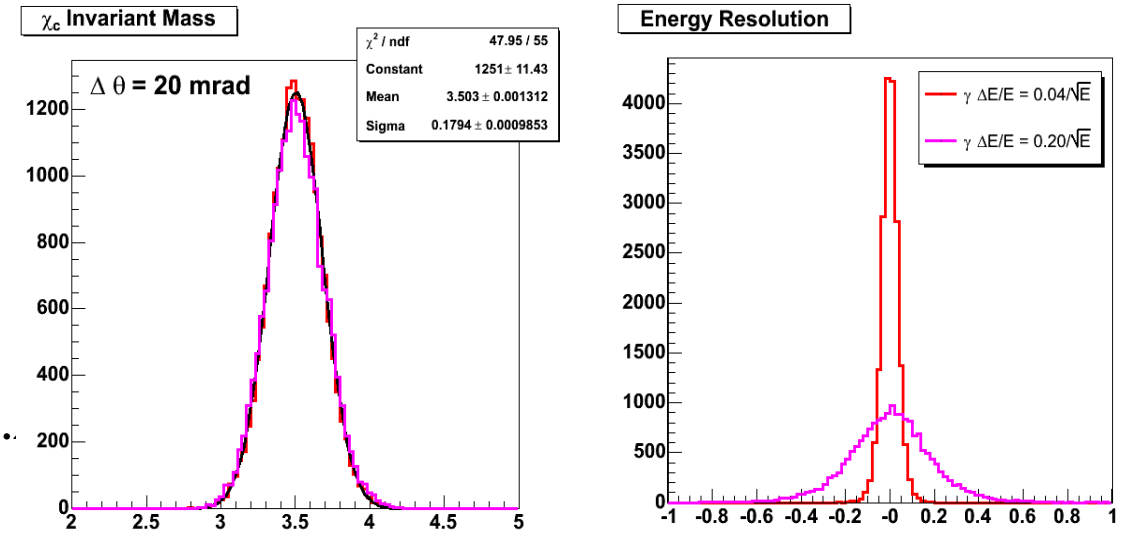

Fig. 15. The invariant mass distribution of reconstructed χ_c with 2 different scenarios for the energy resolution of the NCC (left) and momentum resolution in the muon spectrometer (right).

χ_c with 2 different scenarios for the energy resolution of the NCC and momentum resolution in the muon spectrometer commensurate with the observed J/ψ resolution from Run-3 data at RHIC. The 170 MeV resolution determined by this simulation could be significantly improved with additional measurements by the muon spectrometer of the upstream muon trajectory and the use of a 3 body kinematic fit.

Correlations of direct photons with jets, or high p_T hadrons, will be one of the major goals of the heavy ion program in the coming decade. Since the direct photon will not suffer from energy loss, it will serve as a calibration for the energy loss of its partner parton. One immediate question which arises is whether the calorimeter will be overwhelmed with pile up due to the high occupancy in Au-Au events. Fig. 16 shows a comparison of the expected direct photon signal and pile up photons. We will be able to make such measurements for pseudo-rapidities below 2. Work is on-going to see if this range can be extended. It is important to note that in Au-Au collisions it will be possible to use statistical means to isolate the signal since we are looking for the correlation of the high p_T photon with a jet or high p_T hadron in the opposite direction. Even the addition of pseudo-rapidities between 1 and 2, will increase the acceptance of the PHENIX detector for this all-important signature by a factor of greater that 5, assuming there is a NCC on both muon arms.

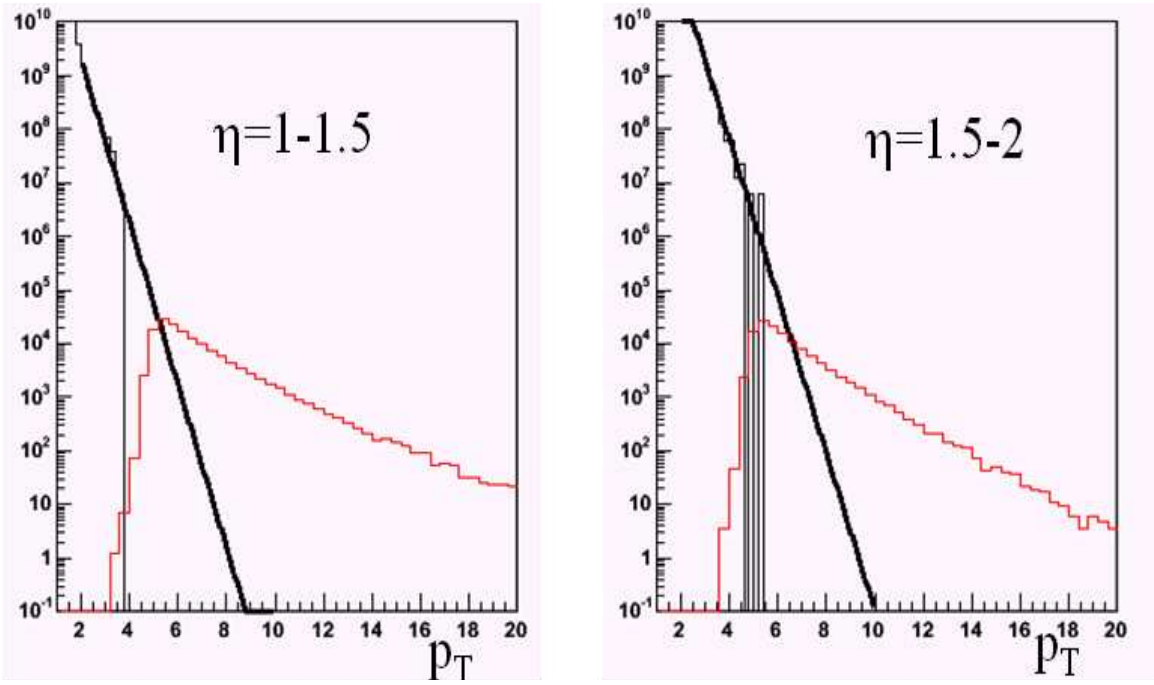

Fig. 16. Distribution of direct photons in central Au-Au collisions (red). The turn on at about 5 GeV is due to a cut off in the simulation. False photons from pile up of several photons in a single calorimeter module are shown in black. The dark black line is an extrapolation of the expected background since the statistics of the simulation was limited.

6.3. p-A Physics

Recently there has been an enormous interest in high energy collisions with nuclei. McLerran has proposed that the initial conditions in heavy ion collisions could be calculated assuming that the gluon distributions at low x are saturated. This is closely related to nuclear shadowing. The gluon saturation calculations may be a way to understand the phenomenon of shadowing in a rigorous and calculable way. It is important to understand gluon nuclear structure functions. Proton nucleus collisions at high energies will enable us to measure quark and gluon distributions in nuclei and will test of whether saturation pictures such as the well known Colored Glass Condensate (CGC) are correct. Proton nucleus collisions give measurements of anti-quark distributions at low-x.

A variety of probes can be used to examine quark and gluon distributions at low x as illustrated in Fig. 17. Direct photon production is a particularly attractive channel to probe gluon distributions. Heavy quark and J/ψ production, also sensitive to gluon distributions can be measured via high momentum leptons. Drell-Yan (DY) production, is sensitive to anti-quark distributions. A probe for the gluon distribution which can be used at lower luminosity is π^0 production. This exploits processes similar to prompt photon production and heavy quark production, in which the photon is replaced by a gluon jet, and heavy quarks are replaced by light quarks. One measures the π^0s from fragmentation. Recently confidence in NLO calculations of this process were gained when a first measurement was made comparing the calculations to data [18].

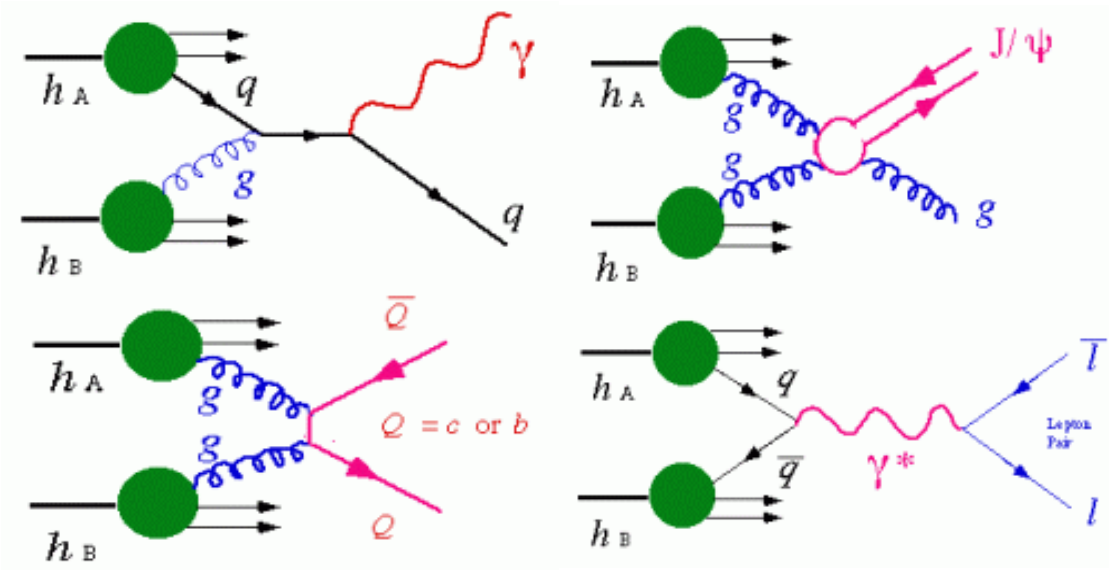

Fig. 17. Diagrams of some of processes to be studied. The first three are sensitive to the gluon distributions and give rise to direct photons, heavy quarks, and J/ . The last diagram can be used to probe anti-quark distributions

6.3.1 Gluon Saturation and Shadowing

In the CGC picture, the gluon distributions at low-x for protons ~1/x violate unitarity at very low x and saturate. This should occur at about $x \sim 10^{-4}$-10^{-5} depending on the Q^2. In a Lorentz contracted nucleus, however, there is essentially a geometric magnification factor of $A^{1/3}$ making the relevant $x \sim 10^{-2}$-10^{-3}. McLerran et al., use a classical approximation to do non-perturbative calculations using renormalization group methods, which depend on a scale Q_s, the saturation momentum, which is around 1-2 GeV/c at RHIC energies. For these calculations Q^2 must be greater than about 1 GeV^2 so that the coupling constant is reasonably small ~0.3 [26]. Saturation is an initial state nuclear property and can be probed using p-A collisions. To observe saturation a measure of the gluon distribution function at very low x is needed. This can be done using a variety of probes. To access the low-x region one must measure at forward and backward rapidities at RHIC energies.

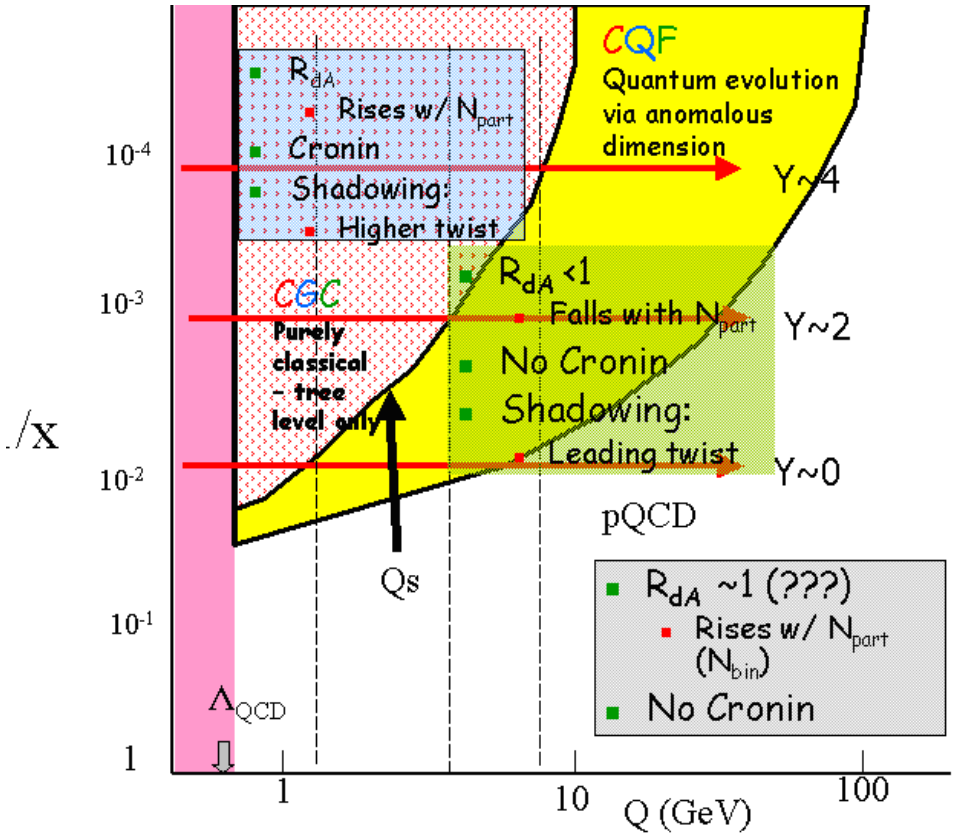

Fig. 18. CGC diagram

A simple diagram of the CGC region and its associated region, the Colored Quantum Fluid (CQF), are shown in Fig. 18. Recent results [27] d-A collisions at RHIC have placed high p_T collisions at central rapidity at RHIC outside these regions, so there is no suppression of high p_T particles in the central region. Multiplicity distributions in Au-Au collisions dominated by low momentum particles appear to be within the region. This is indicated by the lowest red line in the figure which argues that at high p_T, in Au-Au

collisions at RHIC, the suppression of hadrons comes not from saturation effects in the initial state, but from energy loss in the final state. Early data from d-A collisions at higher rapidities indicate that high momentum particles are suppressed indicating that RHIC may be in the CQF region. It thus is important to explore the region between x of 10^{-2} and 10^{-3} to map out the boundaries in the various regions. This can be done by looking at R_{dA} via the measurement of π^0s using the NCC or hadrons, then exploring shadowing effects via the measurement of the gluon structure function using direct photons and open charm/bottom. Recent theoretical work indicates the quark sea should also exhibit these effects, hence a measurement of anti-quark distributions via DY is also important.

6.3.2 Quark Shadowing and p_T Distributions

The phenomenon of nuclear shadowing has a long history [28]. Shadowing in this picture is due to a large coherence length for small x interactions. It was observed in studies of deep inelastic muon-nucleus scattering. There is evidence of nuclear shadowing for the lowest x=0.03 data point of the FNAL Drell-Yan data [29]. Past experiments studying nuclear parton distribution functions (nPDFs) at small x were performed with fixed (stationary) nuclear targets. In these data, the values of x and Q^2 are strongly correlated and one measures nPDFs essentially along a curve in the x-Q^2 plane rather than exploring the entire plane. For $Q^2 > 1$ GeV^2 the data cover the region $x > 5x10^{-3}$ where the effect of nuclear shadowing is just setting in. A feature of all of the calculations is the broadening of the p_T distributions as one approaches the saturation regime by either varying the nuclear species or the centrality of the collision. Another signature of proximity to the saturation would be a significantly weaker dependence of the cross section on the mass of the produced dilepton pair [30].

6.2.3 Particle Production in the Proton Fragmentation Region

The A-dependence of hadron production in the proton fragmentation region remains one of the least understood aspects of hadron-nucleus interactions. Practically all available data are inclusive and indicate that the cross-section is dominated by the production of leading particles at large impact parameters, where the projectile interacts with only one or two nucleons of the nucleus. Thus very little information is available about hadron production at the central impact parameters which are crucial for the study of A-A collisions. Theoretical predictions for this region are also rather uncertain. In eikonal type models, where the energy is split between several soft interactions, one expects a strong decrease of the yield of the leading particles. The dependence is expected to be exponential with path length in the nucleus. But if the valence partons of the projectile do not lose a significant amount of their initial momentum, as suggested by perturbative QCD models [31], the spectrum of leading particles may approach a finite limit for large A and small impact parameters [32]. In this case the leading partons will acquire significant transverse momenta and not coalescence into leading baryons and mesons as it seems to happen in p-p collisions. As a result they will fragment almost independently leading to softer distributions in longitudinal momentum for mesons and especially baryons [32].

Current estimates indicate the strength of the interaction of fast partons in the nucleon (x_p>$10^{-1}$for RHIC) with heavy nuclei at small impact parameters may approach the black body limit for transverse momenta $p_T^{b.b.l.}$<1 GeV/c. Thus all these partons will acquire large transverse momenta ~$p_T^{b.b.l.}(x_A)$. Hence in the black body limit p_T broadening of the partons should be much larger than at low energies where p_T broadening is consistent with the QCD multiple rescattering model [31]. This would lead to a very significant p_T broadening of the spectrum of leading hadrons [33]. Probably the most feasible way to study this effect will be to measure the p_T distribution of the leading hadrons (π^0s) for the collisions at small impact parameters, which will closely follow the p_T distribution of leading quarks [34].

A strong p_T broadening which should increase with increasing x_F clearly distinguishes this mechanism of suppression of the leading hadron spectrum from the soft physics effect of increase of the total p-p cross-section which is rather mild at RHIC energies. Also a very large p_T effect of the leading twist shadowing will tame the increase of the transverse momenta with A. Other interesting topics in p-A collisions include the multiparton correlations in nucleons, and hadron production in the proton fragmentation region.

6.3.4 Physics Goals of the Upgrade

One of the primary goals of this upgrade will be the measurement of the gluon structure functions at low x from $5x10^{-2}$ to 10^{-3} at Q^2 between 1 and 100 GeV^2. Calculations vary between CGC models and other methods of calculating or extracting the structure functions. We would like to measure the full kinematics of the reaction as completely as possible to understand effects such as the intrinsic k_T, which in some models (CGC) can be directly calculated. The extraction of the event-by-event kinematics has inherent complications a variety of processes which include leading order and next-to-leading order processes will contribute. The traditional method of extracting the kinematical variables x_1 x_2 and Q^2 and directly fitting data to extract the parton distribution functions is not the most accurate method because there is no longer a one to one correspondence between experimental measurements such as the energy, angle and momentum and the kinematical variables. Instead we must adapt methods used by groups such as the CTEQ collaboration to fit the experimental distributions to trial parton distributions to extract fit parameters but that does not mean that it is not possible to understand the gluon distributions as a function of these variables. We must rely on NLO pQCD calculations of the processes we measure. Recent comparisons of the NLO π^0 calculation with the measured distribution in p-p give us great confidence in these calculations. Hence we set the following goals:

1) measurement to rapidities of ~3.0 giving a coverage for x_2 down to 10^{-3}.
2) detection of photons and π^0s with discrimination between them in this region.
3) reconstruction of jet direction, and a very crude energy measurement.

4) detection of muons at high rates consistent with luminosities planned for RHIC II.

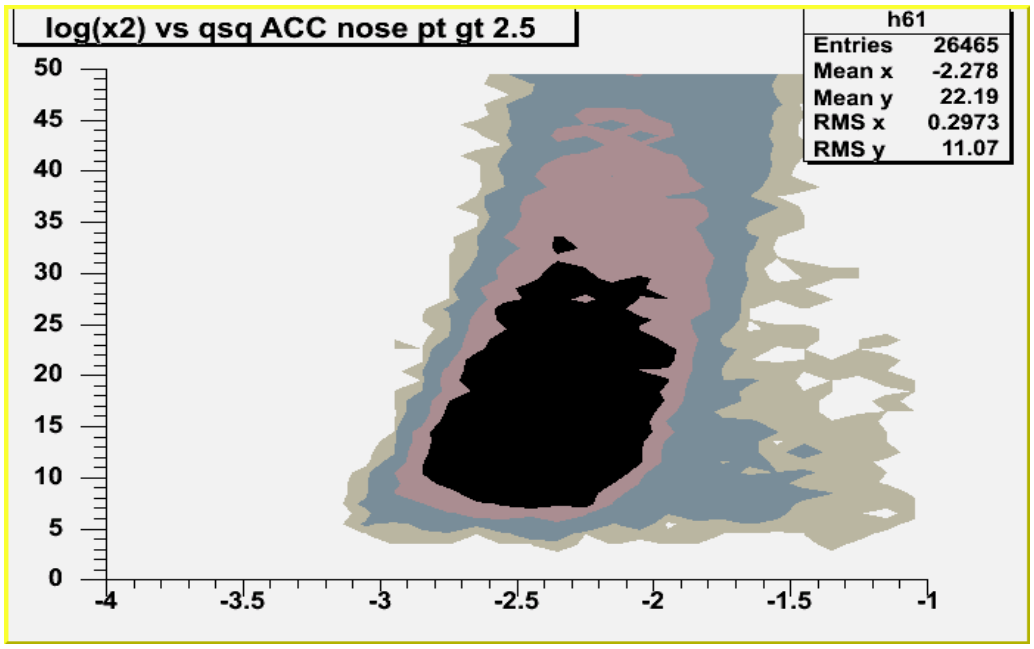

Fig. 19. **C**overage of NCC for direct photon events in 100x100 GeV^2 p-A collisions. The x-axis corresponds to log(x2), the y-axis to Q^2 in $GeV^{2.}$. The contours correspond to the number of events in bins of 0.1 in log(x2), and 1 GeV^2 in Q^2. The contours are 20 events/bin, 100 events/bin, 500 events/bin and 1000 events/bin.

The proposed NCC and muon trigger upgrade gives us access to all processes shown in Fig. 17. It will be important to measure all processes in both p-p and p-A to look for effects unique to nuclei. The production of open charm is particularly suited for this new detector in conjunction with the muon spectrometer, in that we can detect μe events.

To guess the rapidity coverage required, direct photon events were generated with PYTHIA to obtain an estimate of the kinematic range covered with the proposed NCC. The photon was required to have a minimum p_T of 2.5 GeV and rapidity between 0.9 and 3. The results are shown in Fig. 19. The plot corresponds to a 0.5 pb^{-1} p-Au run. There are 4 contours shown which correspond to the number of events in a bin of $\log(x_2)$ and Q^2 of 0.1 x $1GeV^2$. The numerical values for the contours from outside in are 20 events per bin, 100 events/bin, 500 events/bin, and 1000 events/bin. The typical minimum p_T for which one can reasonably identify a direct photon is about 3. Harder cuts on p_T of the photon reduces the coverage. Running at a higher proton energy of 250 GeV rather than 100 GeV assumed for this study helps the situation somewhat. During the design phase careful consideration will have to be given to the various cuts one will need to make to identify the relevant signatures while retaining enough of the signal so that a measurement can be made.

6.4 p-p Physics

A central goal of high-energy nuclear physics is to determine and understand the quark-gluon structure of the nucleon, the fundamental bound state of QCD. The present understanding is largely empirical and rudimentary. A prime example of this is the surprising fact, now well established from inclusive polarized deep inelastic lepton scattering experiments, that only 20-30% of the spin of the nucleon arises from the spins of the quarks. While one would expect a significant contribution from the gluon field, this contribution remains almost completely undetermined. Possible contributions from orbital angular momentum are even less well understood, both experimentally and theoretically, although there are recent hints that this contribution is not small.

The PHENIX experiment, along with the STAR and COMPASS experiments, will make the first direct measurements of the gluon contribution to the nucleon spin, $\Delta G(x)$, over a significant range in momentum fraction x. The basic processes are polarized gluon-gluon and polarized quark-gluon hard scattering leading to different final states, as shown in Fig. 20.

First results from PHENIX Run-3 have already been produced which constrain models with different gluonic spin contributions. With future data acquisition, the variety and power of these measurements will greatly increase. Given these measurements, a fundamental question will be how the quark and gluon contributions mutually arise in the nucleon bound state. In particular, how is the polarization of the sea quarks, which are formed from the gluon field, affected by the polarization of this field. In order to answer this more detailed question, experiments at CERN (SMC, COMPASS) and DESY(HERMES) have and are attempting to determined the spin contributions of the different quark flavors separately, especially the contributions from the sea quarks. The technique used is so-called “hadron tagging” based on the measurement of semi-inclusive asymmetries, in which a leading hadron (*i.e.,* a hadron containing a large fraction of the energy transferred to the nucleon) is detected in coincidence with a deep-inelastically scattered lepton. Using statistical analysis and empirical fragmentation models, one can exploit the greater than random probability that the leading hadron contains the struck quark, and use the hadron species to limit the possible flavor of the struck quark. Measuring concurrently a sufficient number of semi-inclusive asymmetries with identified leading pions and kaons allows an extraction of the spin contributions from the different quark and anti-quark (sea) flavors. The results of the analysis of the HERMES data are shown in Fig. 21.

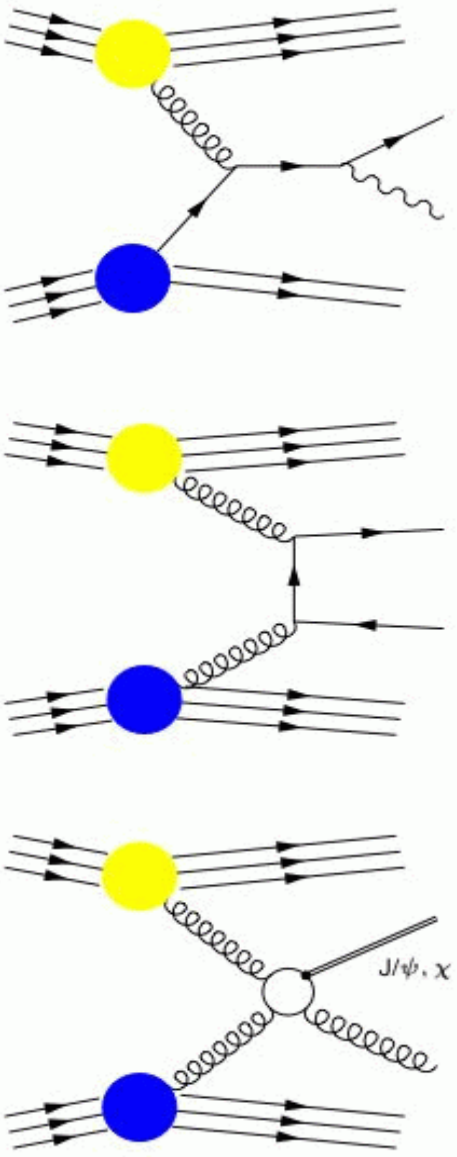

Figure 1.4.1

Fig. 20. Basic processes sensitive to the gluon polarization.

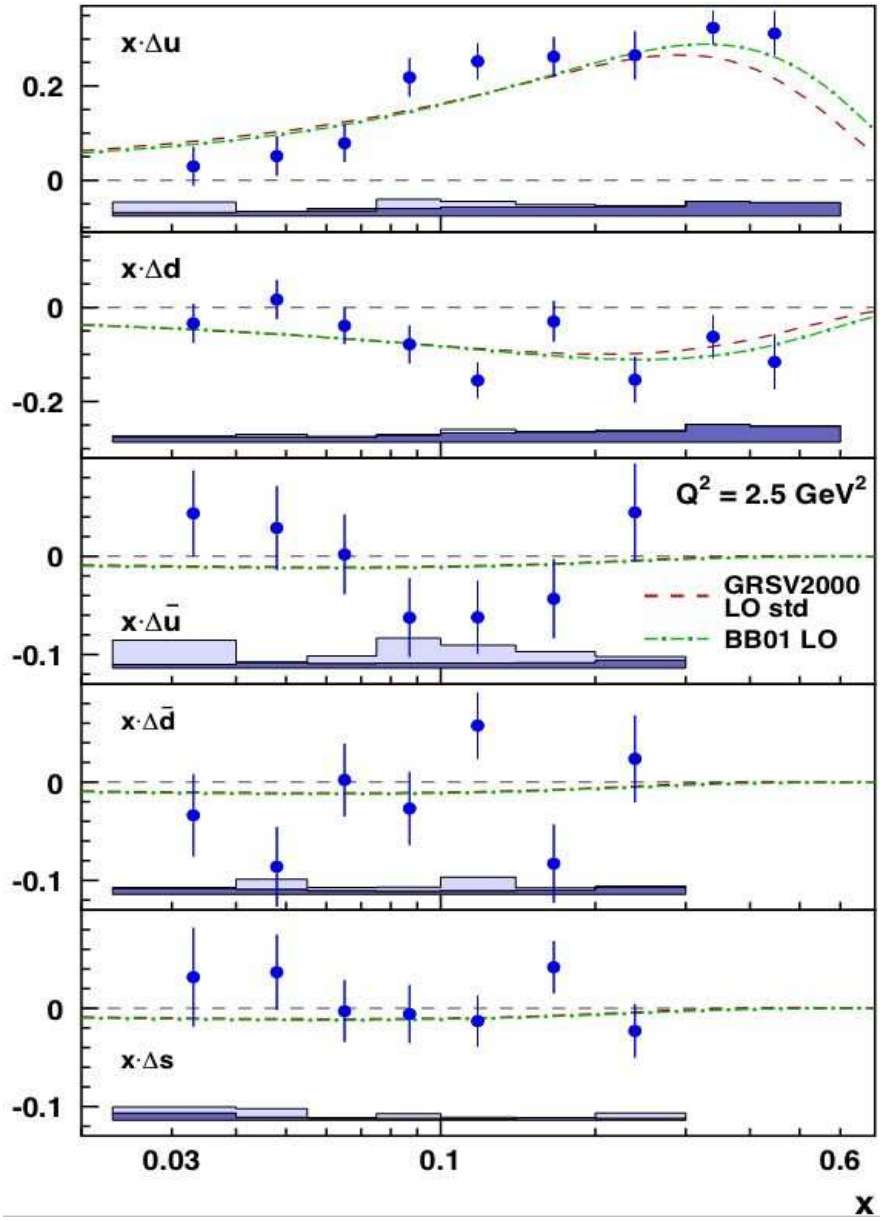

Fig. 21. Results of HERMES spin-flavor decomposition using semi-inclusive deep-inelastic electron scattering [32].

To date, this extraction has only been performed within a leading order (LO) QCD "framework", that is, with the effects of the Q^2 evolution only minimally included and no attempt at inclusion of higher twist effects. Several theoretical programs to extend the semi-inclusive analysis procedure to next-to-leading order (NLO) are underway. A chief concern with the HERMES analysis is the relatively low Q^2 (average about 2.5 GeV^2) of the data, which may result in large NLO corrections. The forthcoming analysis from COMPASS will certainly use a data sample with significantly higher Q^2 which will likely have smaller NLO corrections. Furthermore, it will extend the determination to almost

an order of magnitude smaller x value than HERMES. Because COMPASS only will use a polarized deuterium target, some additional assumptions about the proton and neutron parton distributions will be required. Nonetheless, the HERA collider experiments have shown just how strongly coupled the resolution of the sea distributions are to the Q^2 of the probe, so it remains important to measure the spin-flavor composition of the nucleon up to the highest Q^2 possible.

However, a common systematic uncertainty in the analysis of both experiments is the hadron-tagging technique itself, which relies on the use of fragmentation function models which in some cases (*e.g.,* s quark fragmentation to kaons) are not well known due to a general lack of data, especially at lower energies. While there is hope that new (and voluminous) data from the Belle experiment will significantly improve this situation, there will remain issues related to possible differences in how the fragmentation process occurs starting from the initial quark-antiquark pair in e+e- colliders and the process starting from a quark struck from a nucleon. Furthermore, both COMPASS and HERMES suffer from the "u-quark dominance" caused by the weighting of the fundamental photon-quark interaction by the square of the quark charge. Hence it is difficult to extract precise information about the down and strange quark (and anti-quark) polarized distributions. Since the weak interaction lacks this bias, intense high energy neutrino beams would be ideal for this type of semi-inclusive analysis.

Fig. 22. $W^{+/-}$ production in polarized pp scattering.

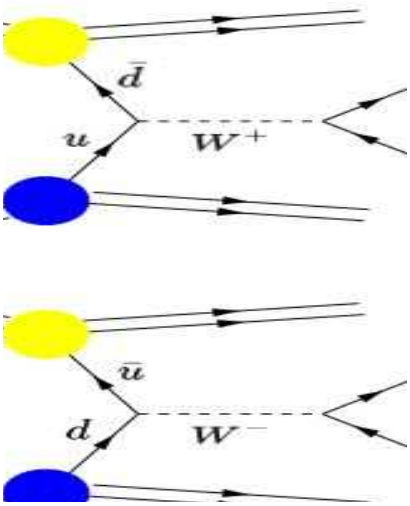

The collision of high-energy polarized protons at RHIC provides a completely new means to use the weak interaction as a probe of the polarized parton distributions, namely $W^{\pm}$ production, leading to a very high energy muon or electron, of the same charge as the W and with an energy of roughly half the W mass, as shown in Fig 22. This measurement and estimates of the sensitivity are described thoroughly in Refs. [33-35], so we here recall the major points. This reaction mechanism offers a number of advantages over deep-inelastic scattering: there are no systematic uncertainties from fragmentation models, there is no u-quark dominance arising from the intrinsic vertex coupling strength, the parity violating nature of the weak interaction provides a natural polarization measurement so that only a single spin asymmetry is required, and the Q^2 of the measurement is very high, essentially at the mass squared of the W boson.

Fig. 23 shows the results of a simulation of the expected statistical accuracy of a measurement for 800 pb^{-1} integrated luminosity, 70% beam polarization, and with the

PHENIX detector assuming the nominal energy and solid angle acceptance. However, it assumes that the rapidity of the W can be determined accurately, whereas in fact, because the neutrino is not detected, one can only determine the decay charged lepton's rapidity and p_T, and then via a statistical analysis relate the rapidity and p_T asymmetries to those of the parent W bosons. These effects and also higher order QCD corrections have been extensively investigated by Nadolsky and Yuan [35].

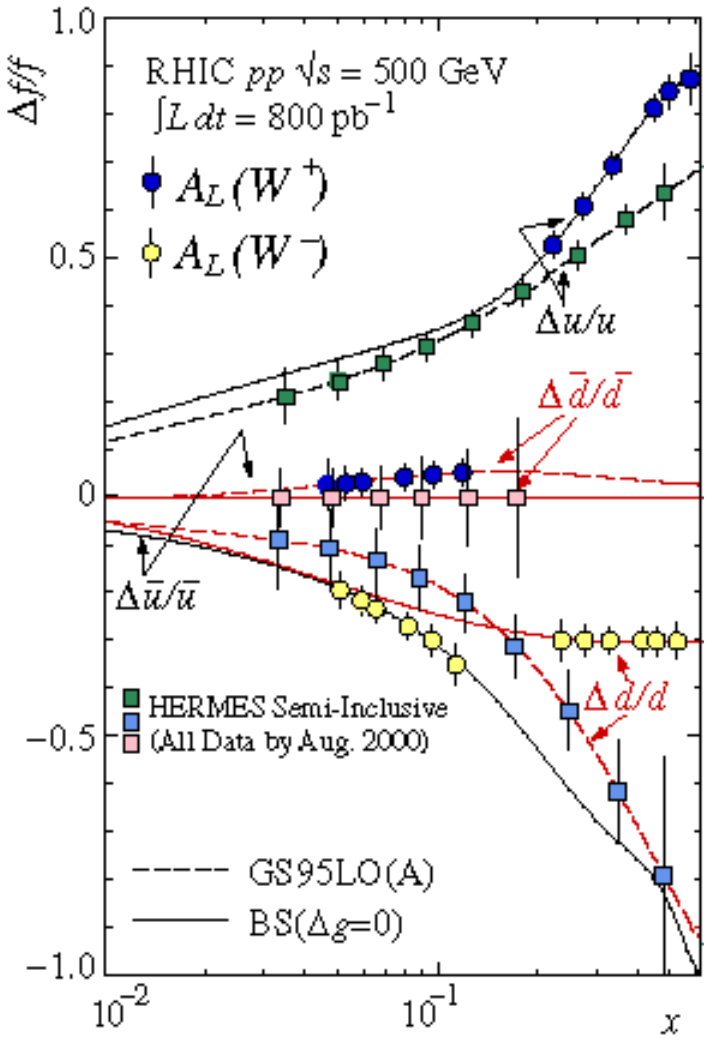

Fig. 23. Expected statistical precision of spin-flavor decomposition using W boson single spin asymmetries.

Since the instantaneous rate of observed W decay leptons is not high, it is critical that the muon trigger have both high efficiency and discrimination. Specifically, it should be sensitive to the higher average momenta of the W decay muons and insensitive to muons

resulting from hadron decay, especially from hard jets. Upgrades introducing muon fast tracking in level one trigger processors combined with nosecone calorimeter information to eliminate hadron jets off-line will provide the information necessary for carrying out the W physics program.

In addition to the studies of the spin-flavor composition of the nucleon, the addition of a nosecone calorimeter opens a new window on the measurement of ΔG through the detection of both the hadron jet and final state photon in the direct photon process. This would extend the capabilities of the PHENIX detector to allow the determination of the momentum fraction x_G of the gluon on an event-by-event basis, similar to that of STAR and more importantly, significantly extends the range of x_G given forward photon detection, roughly down to 0.001 at $\sqrt{s}$ of 200 GeV.

To date, this extraction has only been performed within a leading order (LO) QCD "framework", that is, with the effects of the Q^2 evolution only minimally included and no attempt at inclusion of higher twist effects. Several theoretical programs to extend the semi-inclusive analysis procedure to next-to-leading order (NLO) are underway. A chief concern with the HERMES analysis is the relatively low Q^2 (average about 2.5 GeV^2) of the data, which may result in large NLO corrections. The forthcoming analysis from COMPASS will certainly use a data sample with significantly higher Q^2 which will likely have smaller NLO corrections. Furthermore, it will extend the determination to almost an order of magnitude smaller x value than HERMES. Because COMPASS only will use a polarized deuterium target, some additional assumptions about the proton and neutron parton distributions will be required. Nonetheless, the HERA collider experiments have shown just how strongly coupled the resolution of the sea distributions are to the Q^2 of the probe, so it remains important to measure the spin-flavor composition of the nucleon up to the highest Q^2 possible.

7. Upgrade of the Forward Spectrometer

We discuss here the design and R&D plans for the Nosecone Calorimeter (NCC) and an upgrade option for the level-1 muon trigger. The NCC will occupy the space which is currently used for the nosecone hadron absorbers. The muon trigger upgrade is constrained by the existing muon spectrometer configuration including its wire chambers, hadron absorber walls and magnet yokes. For the muon trigger upgrade we discuss the construction of new dedicated level-1 trigger detectors. The final design will result from ongoing R&D and simulation efforts. Alternate trigger schemes are also being considered. We first discuss plans for the muon trigger upgrade and next plans for the NCC. We plan to submit a detailed proposal for partial funding of the upgrade to the National Science Foundation (NSF) in January 2005.

7.1 Muon Trigger Upgrade

7.1.1 Motivation for the Level-1 Trigger Upgrade

The PHENIX detector initially has been optimized for the needs of heavy ion physics. For high-luminosity p-p and d-A collisions, it is essential to acquire additional low-level event selection capabilities. At full design luminosity for p-p collisions at $\sqrt{s}$=500 GeV the total cross section is 60 mb and the resulting reaction rate is ~12MHz. Therefore powerful level-1 triggers with rejection powers of 5,000 to 10,000 are necessary in order to reduce the high raw collision rates in several rare event trigger channels to levels compatible with the available bandwidth (10 kHz) into the event builder.

At the high rates in p-p collisions, an upgrade of the muon level-1 trigger is required for nucleon structure studies utilizing W-production. The present level-1 muon trigger is based purely on muon chamber identification but the trigger rate is dominated by muons resulting from hadron decays at low momenta, which leads to projected level-1 rates of about 20 kHz. Detailed simulation studies have shown that low-momentum decay muons can be rejected by introducing muon momentum information into the level-1 trigger. We have studied the introduction of new dedicated trigger detectors located upstream and downstream of the muon arm spectrometer magnet. This solution provides sufficiently large rejection levels. In addition to the collisions related muon background from hadron decays the trigger upgrade also has to solve the background problems which arise from beam losses and beam-gas interactions.

It appears that a level-1 trigger based on muon identification, vertex pointing and momentum selection alone may be insufficient to discriminate beam related backgrounds from collision related muons. Assuming that beam related backgrounds in the muon spectrometers are dominated by background particles resulting from incoming beam scraping it will be possible to remove background with a timing cut. A new dedicated

level-1 trigger detector with a timing resolution of a few nanoseconds would provide the required rejection. In this context we are considering scintillator hodoscopes as well as Resistive Plate Chambers (RPCs).

The rejection factor of the present MuID local level-1 trigger has been estimated to be around 250 with Run-3 p-p collision data without shielding. It is significantly lower than the factor 1000 expected from the simulated collision data due to beam related backgrounds. Assuming that the shielding will be perfect and that we can reach the performance seen in simulated data, the rejection factor is still a factor of 10-20 less than that required to satisfy the upgrade requirement. A new level-1 trigger is thus needed.

7.1.2. Upgrade with Dedicated Level-1 Trigger Chambers

A solution to the level-1 muon trigger problem is to introduce new dedicated trigger detectors. Our simulation studies for dedicated level 1-trigger detectors focus on a solution in which Resistive Plate Chambers (RPCs) upstream of MuTr station I and downstream of the MuID provide the required tracking and timing resolution for momentum determination and beam background rejection in the level-1 trigger. RPCs have been introduced at RHIC in the ToF at STAR and PHENIX has decided to utilize RPCs for the planned expansion of the PHENIX ToF. We are investigating using similar RPC technology for the muon trigger upgrade. This will require the development of new FEEs that communicate with a level-1 trigger processor.

Each multi-gap RPC station carries two cathode planes. The first cathode has a coarse tile structure to establish a space point for correlation with the existing muon identifier and the second plane has radial cathode strips in order to provide the required azimuthal angular resolution. The two upstream stations (south and north muon arms) have external dimensions of about 3 m^2 and the total channel count is 1620. The two downstream stations will be located in gap 5 for maximal protection from outgoing beam background. We are studying which area the downstream RPC stations need to cover. Due to the smaller resolution required in the tile structure we expect a channel count lower than in the upstream station of 1120.

Hit and timing information from the RPC stations will be sent through optical fibers to level-1 trigger processors. The trigger processors will be based on the existing Iowa State local level-1 processor. Applications of these processors exist in the MuID, the ZDC and the EMC-RICH trigger. Trigger efficiencies and background rejection factors have been simulated. We find that tile sizes of 10x10 cm^2 in the upstream RPC, 30x30 cm^2 in the downstream RPC and angular resolutions of $\Delta = 1^o$ lead to background rejection factors of 15000-20000 reducing the single muon trigger rates to about 0.5 kHz, well within the available bandwidth.

We have started a R&D project to study the performance of different RPCs at the Univ. of Illinois (UIUC) and RBRC. We have carried out measurements of collision and beam-

related backgrounds during RHIC p-p Run-4. As an immediate application we are considering using the RPCs for a new relative luminosity monitor (RLT) for PHENIX very high luminosity p-p running. Development of detector hardware and readout for the RLT RPCs will be identical to hardware required for the muon trigger RPC. We plan to test different types of RPC s in summer 2004 and build the RLT in 2005.

Collision and beam-related backgrounds will be key factors negatively effecting the trigger performance. Understanding the nature of the backgrounds is important input in determining the final trigger configuration from possible choices. During the 2004 p-p run we measured background in both the central and forward rapidity regions with scintillators. The results will be compared to MARS beam background simulations and will help in calibrating the simulation results. The background rates in different μID gaps have been measured and the MARS simulations show that most of the background seen by the MuID is from slow neutrons absorbed by the PVC used in the MuID Iarooci tubes.

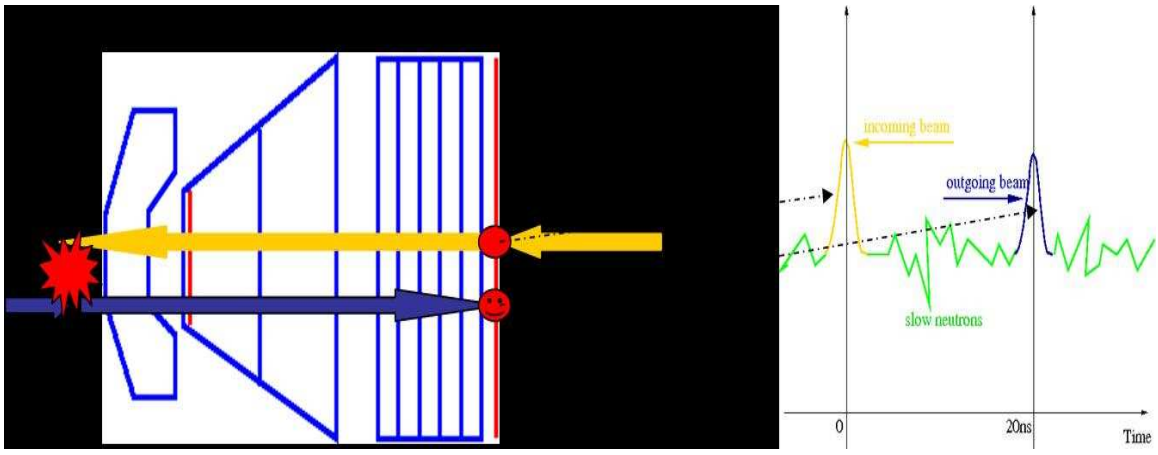

Fig. 24. Timing information can separate incoming beam background from collision related products. Outgoing beam background is in time with collision related products but attenuated by traversing the entire PHENIX detector.

In addition to the neutron background it will be important at higher luminosities to understand background contributions from beam related decay muons. The proposed muon trigger upgrade may have to include new dedicated trigger detectors with sufficient timing resolution to separate collision related products from incoming beam background as illustrated in Fig. 24.

Collision products will occur at the same time as outgoing beam background. We hope to understand the time structure of the background from our 2004 background measurements. In particular it will be important to find out to what extend the material in the PHENIX detector attenuates the outgoing beam background.

7.2 Nosecone Calorimeter (NCC)

7.2.1 Conceptual Design

The physics goals outlined in the preceding chapters place considerable demands on all forward upgrade components, especially the NCC. Reaching all these goals within the envelope of the existing PHENIX magnet nose cones is a challenging task. We describe a reasonable compromise which will allow us to start a physics program on a relatively short time scale and expand it at later stages when all components of a planned detector system will actually become available. A calorimeter will replace the current nosecones in the two PHENIX forward muon spectrometers. They will consist of three laterally segmented longitudinal calorimetry sections (two electromagnetic and one hadronic) built using a common technology (W/Si sampling calorimetry) and a γ/π^0 identifier (orthogonal layers of Si strips) in the space between the two electromagnetic sections.

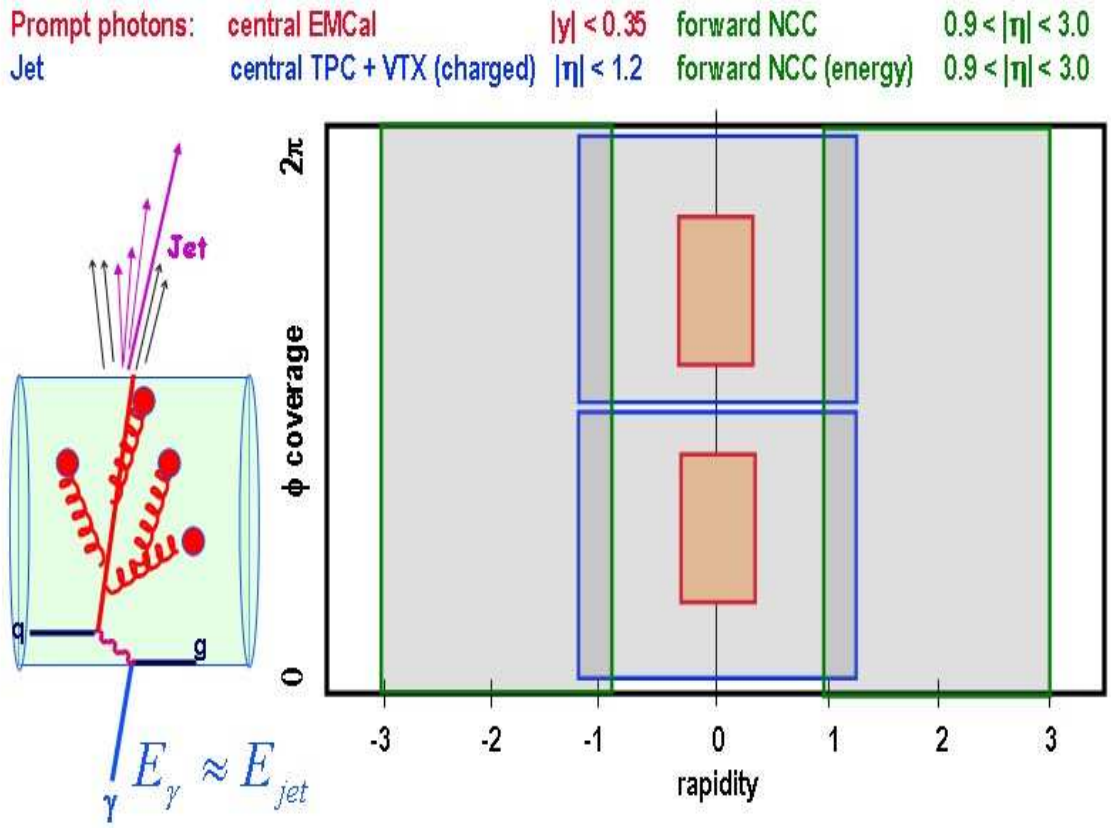

Fig. 25. Comparison of PHENIX rapidity coverage for prompt photons and jets as a function of φ using the central and forward spectrometers. The rapidity coverage in the central region for prompt photons and jets is shown in red and blue, respectively. The rapidity coverage in the forward region is shown in green. A schematic diagram of an interaction leading to both a jet and prompt photon is shown to the left.

A major motivation for the forward detector upgrade is to increase the rapidity coverage for photons and jets in the forward regions. Fig. 25 illustrates the increased rapidity coverage obtained in the upgrade. As shown in the figure the overlap for jet coverage in the forward and central regions is excellent.

7.2.2 Detector Layout and Configuration

The location of the proposed NCC together with the new central tracking detectors is shown in Fig. 26. Available real estate is shared between the forward silicon tracking, the central silicon vertexing system and the tracking TPC. The NCC will occupy the space along the collision axis which is currently used to install supplementary muon filters (nose cones). The depth of the NCC is chosen to fit within the envelope of the existing Nose Cones. We plan to build two identical devices for the North and South Arms of PHENIX.

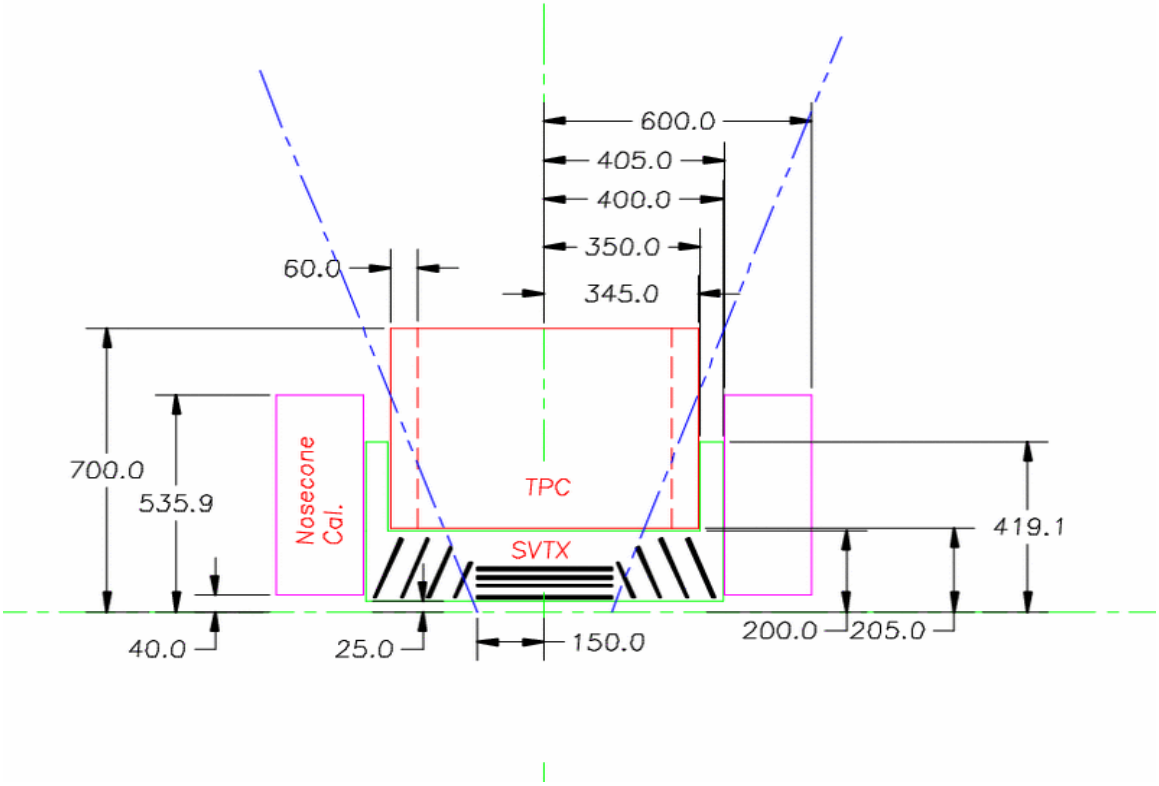

Fig. 26. Sharing of space budget between new detectors in the central PHENIX region.

As a component of the PHENIX Forward Muon Spectrometer the NCC is expected to provide for or contribute to the following:

1) precision measurements of individual electromagnetic showers
2) photon to π^0 discrimination similar to central PHENIX electromagnetic calorimeters
3) photon/hadron discrimination
4) jet finding and jet energy and impact position measurements
5) data for fast triggering

This will require a combination of highly segmented electromagnetic and hadronic calorimeters supplemented by high resolution position detectors located (a) upstream of the calorimeter and (b) at the depth in the calorimeter corresponding to 100% probability for both photons from π^0 decay and are converted and seen in the detector.

We will build the NCC as a super dense sampling calorimeter using an absorber with the shortest possible Moliere radius which is a W/Cu alloy called "heavymet". A few % of Cu is required to allow for easy machining. The choice of a W results in a very short radiation length and a large absorption/radiation length ratio limiting electromagnetic shower development to the very first few cm of absorber. This allows us to implement both the electromagnetic and shallow hadronic compartment within the available space. A γ/π° identifier is located in one of the gaps of the calorimeter to aid the separation of close photon showers from π^0 and to add an additional point for tracking muons. Table1 summarizes the goals of our design and Table 2 shows their implementation.

GEANT simulation of a single electromagnetic shower initiated by an electron with a momentum of 10 GeV/c in this calorimeter is shown in Fig. 27 which clearly illustrates our main design ideas of compact showers, minimal background to electromagnetic energy measurements, reasonable hadronic energy measurements and the ability to reject hadrons with only calorimeter data.

Observable	**Featured parameter**	**Goal**
Photons	EM resolution	~20%
	position resolution	~3 mm to be comparable to central calorimeters
	Hadron rejection	better then 100
Electrons	Upstream tracking	impact position known to better then 1 mm
Muons	Upstream tracking and /or tracking inside NCC	few points on muon trajectory measured with sub mm resolution
Jets	Depth	~2 $_{\text{Absorbtion}}$
	Acceptance	0.9 < < 2.5
	Multiple shower separation	few cm

Table 1. General considerations important to designing the NCC system.

To date, this extraction has only been performed within a leading order (LO) QCD "framework", that is, with the effects of the Q^2 evolution only minimally included and no attempt at inclusion of higher twist effects. Several theoretical programs to extend the semi-inclusive analysis procedure to next-to-leading order (NLO) are underway. A chief concern with the HERMES analysis is the relatively low Q^2 (average about 2.5 GeV^2) of the data, which may result in large NLO corrections. The forthcoming analysis from COMPASS will certainly use a data sample with significantly higher Q^2 which will likely

have smaller NLO corrections.

Parameter	Value	Comment
Beginning Z-coordinate	40 cm	
Radial coverage	50 cm	
Geometrical depth	~20 cm	
Absorber	W	(16 x 2.5 mm + 6 x 16 mm)
Readout	Si pads	Single readout layer is 2.5 mm thick
Sampling cells	22	EMC(16 x 0.5cm) + HAD(6 x 1.85 cm)
Longitudinal segments in readout	3	Summation over 6 – 10 – 6 sampling cells
EM compartment (Rad length)	9	
Total depth (Rad length)	~40	
Total depth (Abs length)	>1.5	
Multiple scattering (MeV) in NCC combined with Fe magnet pole	133	Compared to 106 MeV in the existing configuration with Cu NoseCone
Expected EM energy resolution	20%	
Tower size (cm)	1.5 x 1.5	Nonprojective
Two showers resolved at	3cm	
γ/π° identifier	In gap 6	Two orthogonal layers of silicon strips
γ/π° identifier granularity (mm^2)	2 x 60	
Two showers resolved at	0.3 cm	

Table 2. Concepts for the W/Si Nose Cone Calorimeter

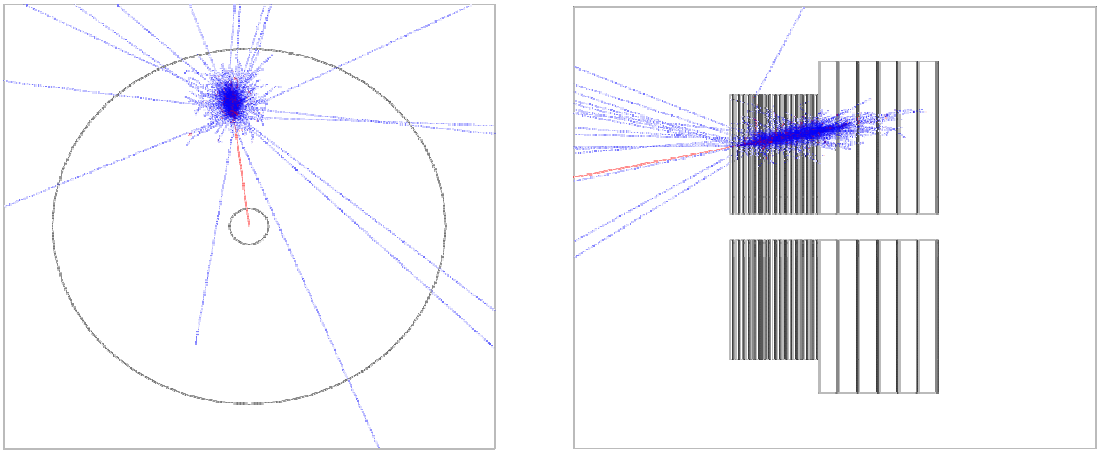

Fig. 27. Front (left) and side (right) views of a 10 GeV electron on the NCC producing an electromagnetic shower. In the left view the electron enters from the lower right.

7.2.3. NCC Event Environment and Effect on Muon Measurements

The NCC is close to the production vertex so the NCC will work at high occupancy. A simple analytical computation of the probability for a sensor (or strip in the SMD) was made assuming the worst possible scenario that any shower in the calorimeter would fire a base matrix of 3x3 towers and 3 neighboring strips in the SMD. The strips and towers were assumed to be of a similar surface area (~200 mm^2). The resulting radial (from the beam) dependence of the probability for strips in the SMD and towers in the calorimeter to see event related energy is plotted in Fig. 28.

In p-p collisions, conditions similar to those in the central calorimeter are reached at a radial distance of 10 cm so the entire calorimeter will have a reasonable occupancy. Running conditions are less favorable in Au-Au collisions where the NCC will be heavily occupied by showers due to soft secondary particles. The SMD occupancy stays relatively low allowing for cluster counting and impact point measurements in the NCC. This permits jet finding based upon hit occupancy in the events of highest multiplicity.

Energy measurements in Au-Au collisions will be strongly affected by the pileup from underlying events resulting in higher threshold values and additional inefficiencies. In this respect the most challenging part of the NCC program is jet measurements. Multiple approaches such as threshold selected hit counting, energy profiling and energy flow which requires tracking the momenta of charged particles will be used. Fig. 29 is a crude example of what to expect in p-p collisions.

Depending on the rapidity, a 4 GeV/c transverse momentum jet in the NCC acceptance window will have a total energy of 8 GeV to 80 GeV. It will be seen in the calorimeter with very little pileup contribution up to ~2.5 units of rapidity and will start merging with the underlying event only at rapidity ~3. In p-p collisions a dense relatively shallow calorimeter will see high p_T jets as easily identifiable, narrow peaks in the energy profile. Due to the background from underlying events in Au-Au collisions, there will be more smearing to the energy profile which will move the threshold for identifiable jets to higher transverse momenta.

One of the goals of the NCC program is to measure the χ_C which decays to a J/ψ and a photon. The resolution of this state is primarily dictated by the resolution of the J/ψ. GEANT was used to estimate J/ψ resolution in the absence off multiple scattering (due to Landau fluctuations and measurement errors) equal to 118 MeV. The contributions due to the multiple scattering were estimated by subtracting this value quadratically from the J/ψ total width and is equal to 100 MeV. An estimate based upon the number of radiation lengths of material in 19 cm Cu and 60 cm Fe (magnet pole) gives 106 MeV for

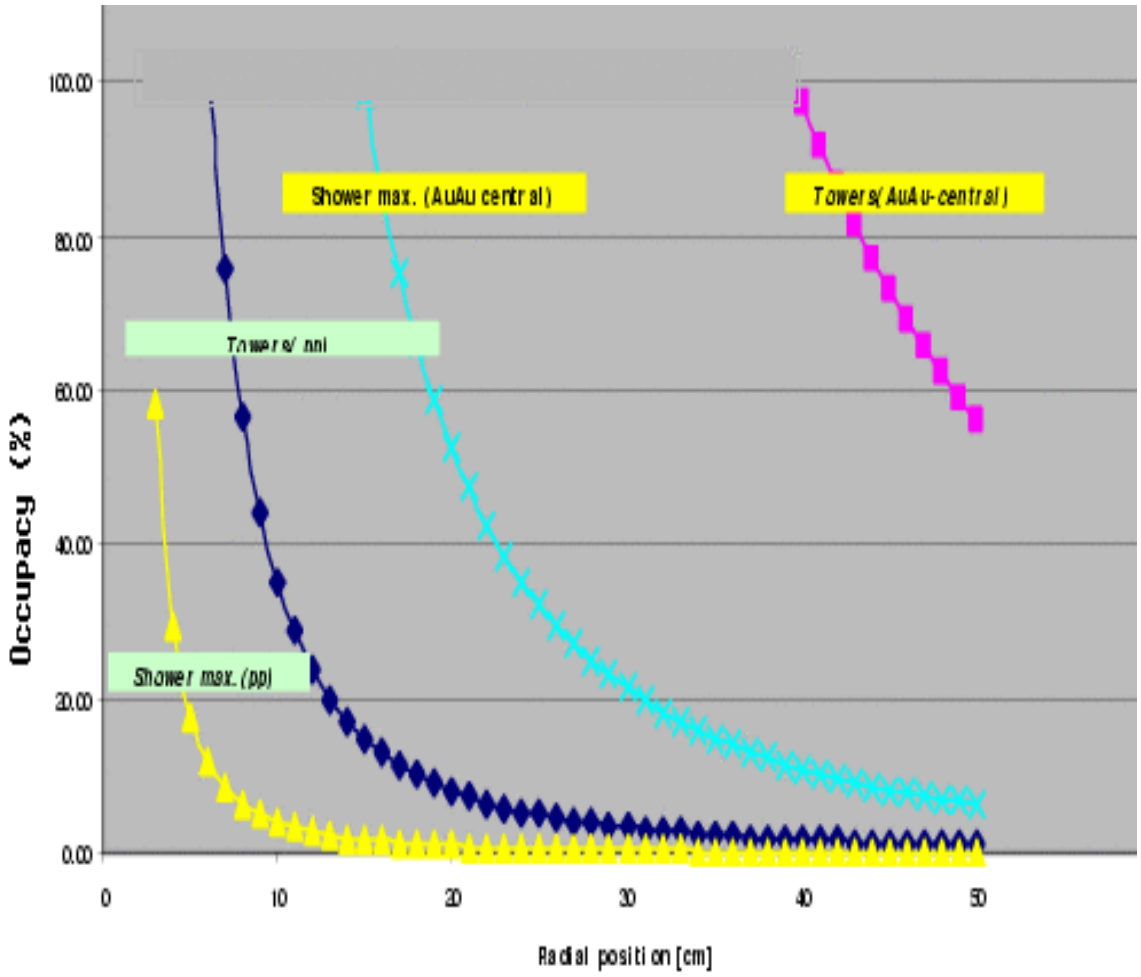

Fig. 28. Probability for tower in NCC and strip in SMD to be fired in Au-Au collisions in PHENIX as function of the distance from the beam pipe.

the same value. The corresponding estimate for the NCC calorimeter is 133 MeV leaving the straggling contribution almost unaffected. The same GEANT simulation has shown a 5% loss in the number of reconstructed J/ψ consistent with expectations due to 200 MeV increase in the momentum cutoff due to ionization losses.

Replacing the existing Cu nosecone with the NCC will add 23 MeV to the J/ψ width, if no effort is made to use the SMD and/or forward Si to improve J/ψ mass resolution. While straggling contributes to muon momentum uncertainties, multiple scattering is responsible for angular (or muon transverse momentum) measurement uncertainties. If muon trajectories upstream and downstream of the major scatterer (Fe magnet pole) are matched and the muon directional vectors measured upstream are used to compute the J/ψ effective mass, the multiple scattering contribution can basically be eliminated. This approach will certainly work in p-p collisions. Testing its efficiency in Au-Au central events will require further simulation.

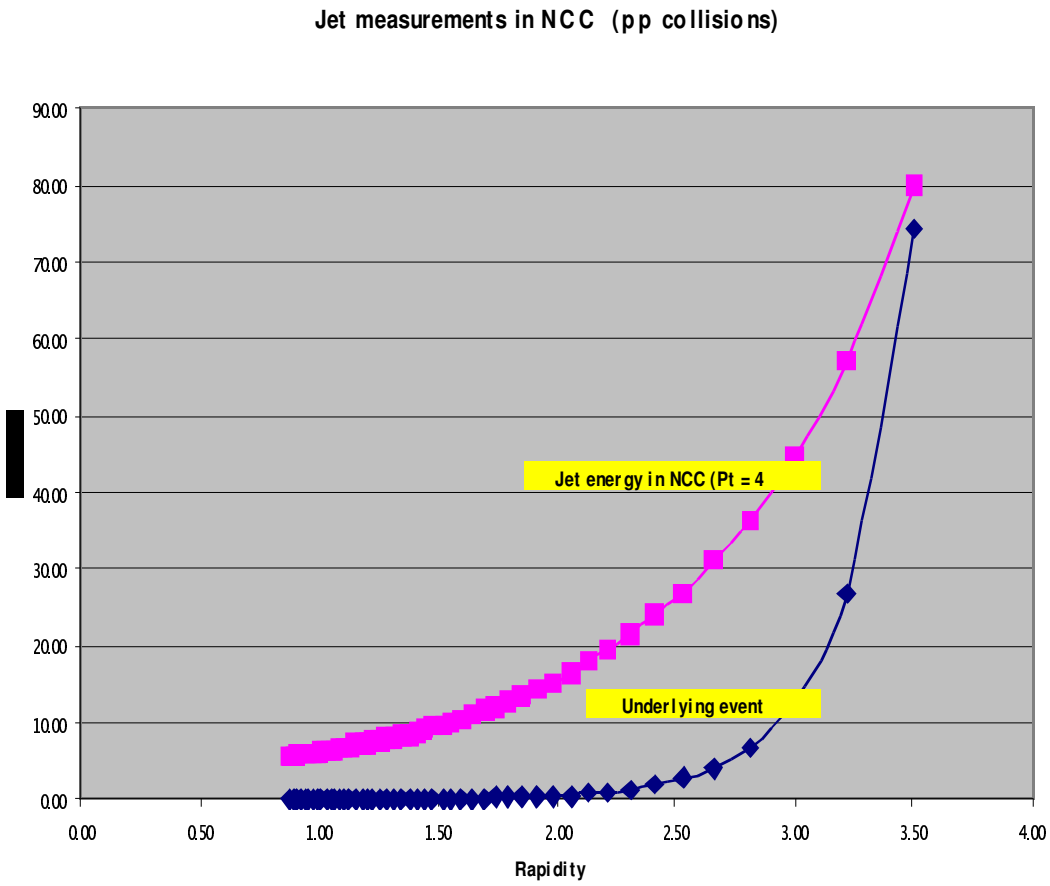

Fig. 29. Effect of the underlying event on jet measurements in the NCC in p-p collisions.

7.2.4. FEE (Readout, Signal Packaging and Processing)

For readout purposes the NCC is longitudinally segmented into two fine and one coarse sections (two electromagnetic and one shallow hadronic compartments), however the current readout concept is very fluid based upon what is known about similar calorimeter detectors elsewhere. The Si-W calorimeter described above section will have close to 80000 Si pixels demanding a compact, economical readout. We thus seek an integrated solution, where one channel of electronics serves a large number of pixels and the electronics is compatible with the NCC mechanical structure and other components of the PHENIX central detector upgrade. Modest requirements on energy resolution in the NCCs makes digitization of signals from individual pixels unnecessary. We opt for passive summation of the amplified currents due to shower signals in sequential detector layers.

Fig. 30 illustrates two different approaches to the initial stage of signal amplification. We currently consider DC (all current handled in the input amplifier) and AC (using bypass capacitor coupled detector pixels). The DC coupled diodes could be used only if we are certain that the current limit set by the readout chip design (reasonable assumption of 100 nA per channel) is never reached.

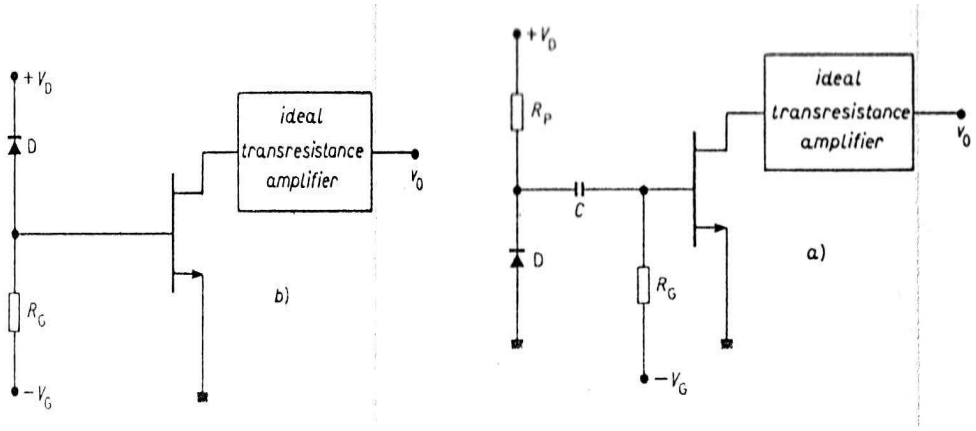

Fig. 30. Two approaches to signal processing are shown.

We consider the case of the total fluence of 100 kRad(Si) or about $3x10^{12}$ equivalent neutrons/cm^2. For a pad size of the order of a few cm^2 and 300 mkm sensor thickness, published data predicts the leakage current of the order of 5 – 10 mkA per pad or at least an order of magnitude higher than desirable. To avoid the potential of failure we propose to use AC coupled sensors in the NCC. This decision is unusual for pad sensors, since all large area sensors currently used in calorimetry are DC coupled devices connected to preamplifiers via blocking capacitors. Extreme space constraints of the PHENIX geometry force us to opt for an integrated solution which is the only available approach to avoid mounting 16 high voltage (relatively large) capacitors per sensor on every readout unit.

We will sum up 6, 10 and 6 depth-sequenced pixels in the first, second and third longitudinal sections of the calorimeter. We will use custom flexible cables with a layout similar to the readout unit motherboard layout. It is typical for similar applications to have one end of this cable to serve as an extension to the outer edge of the readout units. Another end of the cable will be plugged into the zero insertion force connector on the adapter/sumer board positioned in close proximity to the detector. Given the density of the lines on the edge of the readout unit we are not planning for any connectors on the readout unit itself . Rather modest goals for the electromagnetic energy resolution allow us to disregard the potential contribution to resolution due to the spread in the gains between individual channels and/or preamplifier chips. Summing up the amplified currents allows us to control the capacitive noise due to the increased detector capacitance.

Each readout unit will deliver 256 signal lines to an adapter board. The number of lines in use will depend on the unit location in the detector and can be as low as 160 for the top and bottom rows. We are planning to use the same design everywhere for the adapter boards, 352 boards in total, each sending 256 summed outputs to signal processing and trigger logic electronics.

7.3. Local Level-1 Trigger Electronics

In order to pursue it's rare-event physics program the PHENIX experiment requires high luminosity from the RHIC accelerator and highly selective level-1 and level-2 trigger systems. The level-1 trigger system [11] is limited to a maximum rate of 12.5kHz by the readout rate of the detector FEEs. An overall event rejection of up to ~1000 will be needed when RHIC reaches its goal of ten times design luminosity for protons. Since we anticipate the parallel acquisition of several rare event channels, the rejection for an individual trigger channel must be larger by a factor 5-10. The level-1 trigger provides an event decision in less than 4.2 μs. The PHENIX level-1 trigger is a parallel, pipelined trigger that is highly configurable. It consists of two separate subsystems. The Local Level-1 (LL1) systems communicate directly with the participating detector systems and process data to produce a set of reduced-bit input primitive data for each RHIC beam crossing. The Global Level-1 (GL1) system combines this data to provide a trigger decision. Busy signals are managed by GL1 and the trigger communicates with the PHENIX timing and control system via a Granule Timing Module (GTM). The GTMs distribute the local 9.4 Mhz RHIC beam clock as well as control bits and event accepts to the subsystems.

In the PHENIX upgrade the NCC LL1 primitive system will generate information on the jet axis, as well as single and multiple high energy clusters. A possible MuTr LL1 system will generate information on the momentum of high p_T tracks. The MuID LL1 system is based on a generic, configurable LL1 trigger board designed and built by Iowa State Univ. The Generic Local Level-1 (GenLL1) was designed to address a number of difficulties faced in extending the original design concepts for LL1 systems to address the full range of PHENIX trigger needs. The hardware is reprogrammable to allow not only quick corrections to the trigger logic but modifications of the trigger system. It can manage a data throughput of ~20 Gb/s in order to be able to handle large data volume detectors without prohibitive cross-stitching between multiple boards. Also to minimize power consumption and heat load on the board the GenLL1 design used the next generation of HP GLINK receiver/transmitter logic (the HDMP 1032/1034), which runs at 3.3V. Smaller format transceivers (Agilent HFBR 5912) were used to handle up to twenty fiber inputs on a single 9U VME board. A complete description of the GenLL1 hardware can be found elsewhere [39].

In order to maximize the trigger rejection at level-1 it will be necessary to combine trigger information from all of the forward level-1 systems. In order to accomplish this, a

new regional trigger processor will take the trigger primitive information from the NCC, μTr and μID, combine the individual detector LL1 primitives, make trigger decisions and send them to GL1. A block diagram of the data flow is shown in Fig. 31. In order to pass data between the regional trigger processor and the LL1 systems efficiently it may be possible to locate all the level-1 trigger systems in a single crate and make use of a high-speed 16-bit data bus already available in the GenLL1 design to transfer the trigger primitives.

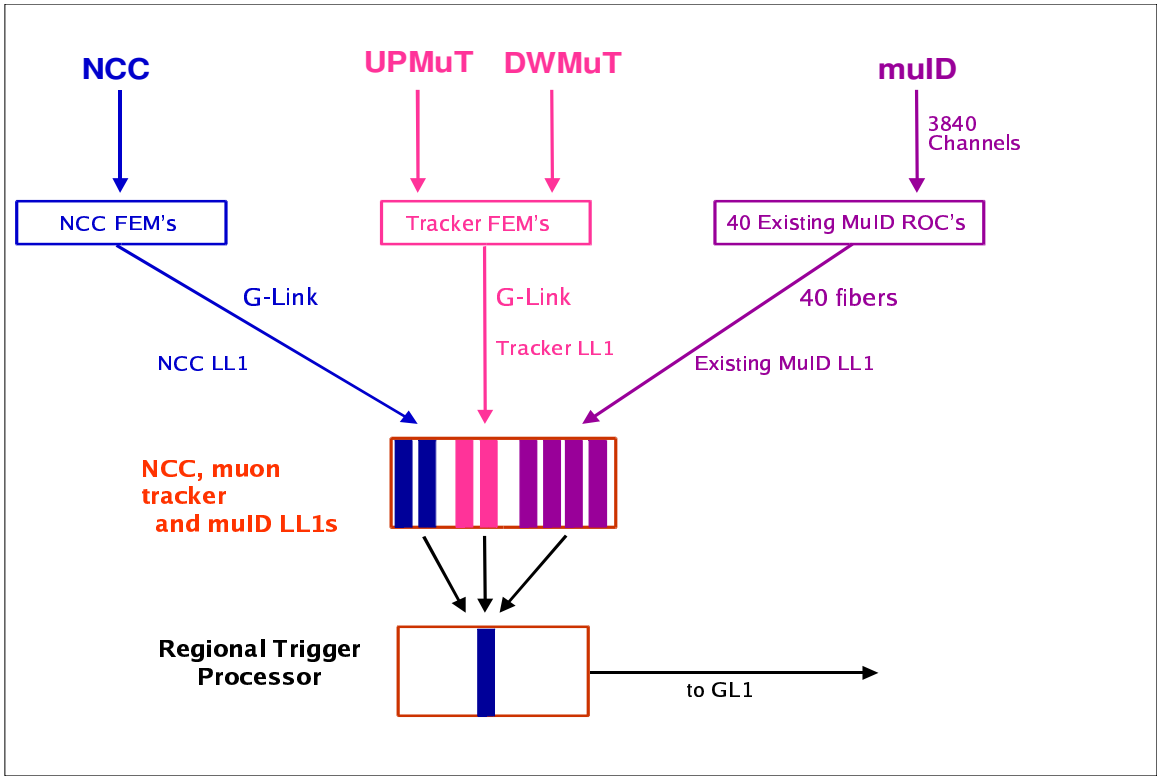

Fig. 31. Block diagram of combined forward PHENIX level-1 trigger system showing the NCC, trigger MuTr stations and the existing MuID LL1 system for a single PHENIX muon arm. In order to combine the primitives of the various trigger systems a regional trigger processor will combine the trigger information before sending primitives to GL1.

7.3.1. The NCC Level-1 Trigger System

The NCC will use a LL1 trigger to select events via with a high p_T photon or jet in the calorimeter acceptance. The processing will consist of a set of pipelined stages. First primitive data will be digitized on the FEMs. Second, this data will be transferred to an LL1 system, and finally the bit-reduced trigger information will be sent to the GL1 trigger, possibly via a new regional trigger processor combining level-1 information from the different forward detector systems.

The NCC system consists of over 10k channels of analog data per nosecone spread over three layers in depth. The FEMs will combine calorimeter towers into non-overlapping

2x2 trigger tiles, digitize the output, and pass the LL1 system an 8-bit ADC value per trigger tile. The 8 bits per channel will allow a ~400 MeV least count with a full range of 100 GeV, and will result in an aggregate bandwidth of 200 Gbit/s per nosecone into the LL1 system, roughly a factor of 5 times larger than the data processing capacity of the existing MuID LL1 system.

We are considering transferring the data over high-speed serial links into an LL1 system located in the detector hall as opposed to other LL1 systems that transmit their data over optical fiber links to LL1 electronics in the PHENIX rack room. The advantage of this approach would be that with serial links we could concentrate the entire NCC LL1 data stream into a smaller number of LL1 modules simplifying the data cross-stitching required for jet cluster trigger algorithms. This would only be possible by using high-speed copper serial links between the detector FEMs and the LL1 electronics which are inherently short-range, requiring the LL1 electronics to be located in the detector hall.

The LL1 system would process the NCC 2x2 data to provide a set of photon triggers and jet cluster triggers based on the 2x2 trigger tiles where both sets of algorithms would operate both laterally and use the NCC depth information to provide clean photon triggers. Detailed simulations of the performance of the NCC LL1 system are underway. The reduced bit output of the NCC LL1 trigger, in the form of a set of bits indicating satisfied algorithms, would be transmitted to the GL1 system over optical fiber.

References

[1] H. Hahn et al., Nucl. Instr. and Meth. A 499 (2003) 245.
[2] I. Alekseev et al., Nucl. Instr. and Meth. A 499 (2003) 392.
[3] K. Adcox et al., Nucl. Instr. and Meth. A 499 (2003) 469.
[4] C. Adler et al., Nucl. Instr. and Meth. A 499 (2003) 433.
[5] M. Allen et al., Nucl. Instr. and Meth. A 499 (2003) 549.
[6] S.H. Aronson et al., Nucl. Instr. and Meth. A 499 (2003) 480.
[7] L. Aphecetche et al., Nucl. Instr. and Meth. A 499 (2003) 521.
[8] K. Adcox et al., Nucl. Instr. and Meth. A 499 (2003) 489.
[9] M. Aizawa et al., Nucl. Instr. and Meth. A 499 (2003) 508.
[10] H. Akikawa et al., Nucl. Instr. and Meth. A 499 (2003) 537.
[11] S.S. Adler et al., Nucl. Instr. and Meth. A 499 (2003) 560.
[12] S.S. Adler et al., Nucl. Instr. and Meth. A 499 (2003) 593.
[13] J. Ashman et al., Phys. Lett. B 202 (1988) 603.
J.J. Aubert et al., Phys. Lett. B 123 (1983) 275.
[14] P. Kolb et al., Nucl. Phys. A 696, (2001) 197.
[15] K. Adcox et al., Phys. Rev. Lett. 86, (2001) 3500.
[16] K. Adcox et al., Phys. Rev. Lett. 88, (2002) 022301.
[17] S.S. Adler et al., Phys. Rev. Lett. 91, (2003) 072303.
[18] S.S. Adler et al., Phys. Rev. Lett. 91, (2003) 241803.
[19] B.A. Kniehl et al., Nucl. Phys. B597, (2001) 337.
[20] S. Kretzer, Phys. Rev. D 62, (2001) 054001.
[21] S.S. Adler et al., submitted to Phys. Rev. Lett.
[22] T. Matsui and H. Satz, Phys. Lett. B 178, (1986) 416.
[23] D. Kharzeev and H. Satz, Phys. Lett. B 366, (1996) 316.
[24] M.J. Leitch et al., Phys. Rev. Lett. 84, (2000) 3256.
[25] B. Kopeliovich, A. Polleri and J. Hufner, Phys. Rev. Lett. 87, (2001) 112302.
[26] L.D. McLerran and R. Venugopalan, Phys. Rev. D 49, (1994) 3352.
[27] S.S. Adler et al.,[PHENIX Collaboration], Phys. Rev. Lett. 91, (2003) 072303;
I. Arsene et al [BRAHMS Collaboration], arXiv:nucl-ex/0403005;
M. Liu et al., [PHENIX Collaboration] arXiv:nucl-ex/0403047
[28] G. Piller and W. Weise, Phys. Rept. 330, (2000) 1.
[29] P.L. McGaughey, J.M. Moss, J.C. Peng, Ann. Rev. Nucl. Part. Sci. 49, (1999) 217.
[30] L. Frankfurt and M. Strikman, Phys. Rev. Lett. 91, (2003) 022301.
[31] R. Baier, D. Schiff and B.G. Zakharov, Ann. Rev. Nucl. Part. Sci. 50, (2000) 37.
[32] A. Berera et al., Phys. Lett. B403 (1997) 1.
[33] A. Dumitru and J. Jalilian-Marian, Phys. Rev. Lett. 89, (2002) 022301.
[34] A. Dumitru, L. Gerland and M. Strikman, arXiv:hep-ph/0211324.
[35] A. Airapetian et al., Phys. Rev. Lett. 92 (2004) 012005.
[36] C. Bourrely and J. Soffer, Phys. Lett. B 314 (1993) 132.
[37] G.Bunce, N.Saito, J.Soffer, W.Vogelsang, Ann. Rev. Nucl. Part. Sci. 50 (2000) 525.
[38] P.M. Nadolsky and C.P. Yuan, Nucl. Phys. B 666 (2003) 31.
[39] J. Lajoie et al., IEEE Nucl. Sci. Sci., N83x, (2002) 534.